JPL D-13399, Rev.B

Earth Observing System

Multi-angle
Imaging
Spectro-
Radiometer

Level 1 In-flight Geometric Calibration Algorithm Theoretical Basis

Veljko M. Jovanović[1]
Michael M. Smyth
Jia Zong

[1]Jet Propulsion Laboratory, California Institute of Technology

JPL
Jet Propulsion Laboratory
California Institute of Technology

March 30. 1999

JPL D-13399

Multi-angle Imaging SpectroRadiometer (MISR)

Level 1 In-flight Geometric Calibration Algorithm Theoretical Basis

Approvals:

David J. Diner

MISR Principal Investigator

Graham W. Bothwell

MISR Science Data System Manager

Terrence H. Reilly

MISR Project Manager

Jet Propulsion Laboratory
California Institute of Technology

Table of Contents

GLOSSARY OF ACRONYMS

B

BIH.....Bureau International de l'Heure

C

CCS.....Camera Coordinate System
CGM.....Camera Geometric Model
CTR.....Conventional Terrestrial Reference

D

DAAC.....Distributed Active Archives Center
DCS.....Detector Coordinate System
DEM.....Digital Elevation Model
DID.....DTED Intermediate Dataset
DMA..... Defense Mapping Agency
DTED.....Digital Terrain Elevation Model

E

ECS.....EOSDIS Core System
EIP.....Experiment Implementation Plan
EOS.....Earth Observing System
EOSDIS.....EOS Data and Information System

F

FOV.....Field Of View

G

GCD.....Geometric Calibration Dataset
GCI.....Geocentric Inertial
GCP.....Ground Control Point
GIIS.....General Instrument Interface Specification
GSFC.....Goddard Space Flight Center

I

ICS.....Instrument Coordinate System
IDQI.....Image Data Quality Indicator
IFDR.....Instrument Functional and Design Requirements
IGC.....In-flight Geometric Calibration

J

JPL.....Jet Propulsion Laboratory

L

L1B2.....Level 1B2

M

MISR.....Multi-angle Imaging Spectro-Radiometer

O

OCC .....Optical Characterization Chamber

OCS.....Orbital Coordinate System

P

PGS .....Product Generation System

PP .....Projection Parameters

R

ROI.....Reference Orbit Imagery

S

SCF .....Science Computing Facility

SCS .....Spacecraft Coordinate System

SOM.....Space Oblique Mercator

U

UIID .....Unique Instrument Interface Document

W

WGS84.....World Geodetic System 1984

1.0 INTRODUCTION

1.1 IDENTIFICATION AND PURPOSE

This Level 1 In-flight Geometric Calibration Algorithm Theoretical Basis (ATB) document describes the concept and underlying theoretical basis used for geometric calibration of the Multi-angle Imaging SpectroRadiometer instrument and production of the Geometric Calibration Dataset (GCD) which is required as an input to the Level 1B2 (L1B2) standard processing. In particular, this document describes characteristics of the required input data, provides the mathematical background underlying the usage of ground control data in order to calibrate the MISR cameras in geometric sense.

1.2 SCOPE

This document covers the algorithm theoretical basis for the parameters to be included in the Geometric Calibration Dataset This dataset is to be generated at the MISR Science Computing Facility (SCF), and then delivered to the DAAC for usage during routine processing of MISR data.

This document is divided into four sections. Section 1 provides the identification, purpose, and scope for the document and lists MISR Project documents and other EOS reference documents which are relevant to the in-flight geometric calibration algorithm. Section 2 provides a technical background. Section 3 gives a theoretical description of the algorithm underlying production of the GCD. References to publications cited in the text are provided in Section 4.

1.3 ALGORITHM DEVELOPMENT AND IMPLEMENTATION

Details describing development strategy, test and validation approaches, and operational design to be used for in-flight geometric calibration are given in the "In-flight Geometric Calibration Plan (JPL D-13228)" document.

1.4 APPLICABLE MISR DOCUMENTS

1.4.1 Controlling Project Documents

[M-1] MISR Experiment Implementation Plan (EIP), vols. 1 and 2 (Instrument), JPL D-8796.

[M-2] MISR Experiment Implementation Plan (EIP), vols. 3 and 4 (Science, Data Processing, and Instrument Operations), JPL D-11520.

[M-3] MISR Instrument Science Requirements (ISR), JPL D-9090, Rev. B.

[M-4] MISR Instrument Functional and Design Requirements (IFDR), JPL D-9988, Rev. A.

[M-5] MISR Data System Science Requirements (DSSR), JPL D-11398.

[M-6] MISR Data Product Description (DPD), JPL D-11103.

1.4.2 Reference Project Documents

[M-7] MISR Level 1 Radiance Scaling and Conditioning Algorithm Theoretical Basis: JPL D-11507, Rev. B.

[M-8] MISR Level 1 Ancillary Geometric Product Algorithm Theoretical Basis: JPL D-13400.

[M-9] MISR Level 1 Cloud Detection Algorithm Theoretical Basis: JPL D-13397.

[M-10] MISR Level 1 Georectification and Registration Algorithm Theoretical Basis: JPL D-11532, Rev. B.

[M-11] MISR Level 2 Cloud Detection and Classification Algorithm Theoretical Basis: JPL D-11399, Rev. B.

[M-12] MISR Level 2 Top-of-Atmosphere Albedo Algorithm Theoretical Basis: JPL D-13401, Rev. B.

[M-13] MISR Level 2 Aerosol Retrieval Algorithm Theoretical Basis: JPL D-11400, Rev. B.

[M-14] MISR Level 2 Surface Retrieval Algorithm Theoretical Basis: JPL D-11401, Rev. B.

[M-15] MISR Algorithm Development Plan, JPL D-11220.

[M-16] MISR Experiment Overview, JPL D-13407.

1.4.3 Other Reference Documents

[M-17] General Instrument Interface Specification (GIIS), GSFC 420-03-02, 1 Dec. 1992, Rev. A.

[M-18] Unique Instrument Interface Document (UIID): MISR Instrument, EOS-AM Project, GSFC 421-12-13-02.

[M-19] (PGS Toolkit Users Guide for the ECS Project, EOSDIS Core System Project, 333-CD-003-002, August 1995.

[M-20] Requirements Document for the EOS-AM Spacecraft, GSFC 421-10-01.

2.0 MISR GEOMETRIC PROCESSING

2.1 INTRODUCTION

The Multi-angle Imaging SpectroRadiometer (MISR) is part of an Earth Observing System (EOS) payload to be launched in 1998. The purpose of MISR is to study the ecology and climate of the Earth through the acquisition of systematic, global multi-angle imagery in reflected sunlight. The instrument flies in a sun-synchronous 705-km descending polar orbit, and is capable of global coverage every nine days. MISR will acquire multi-spectral images at nine discrete angles relative to the local vertical. Four of the nine push-broom cameras are pointed forward of the spacecraft position, one pointed at nadir, and four pointed in the aftward direction.

In order to derive geophysical parameters such as aerosol optical depth, bidirectional reflectance factor, and hemispheric reflectance, measured incident radiances from all nine cameras must be coregistered. Furthermore, the coregistered image data must be geolocated in order to meet experiment objectives such as: a) produce a data set of value to long-term monitoring programs and allow intercomparassions of data on time scales exceeding that of an individual satellite, and b) provide EOS synergism, and allow data exchange between spacecraft instruments. Ultimately, the Georectified Radiance Product (GRP) resulting from the L1B2 standard processing of radiometrically corrected MISR imagery must satisfy coregistration and geolocation requirements imposed by the science algorithms. The GRP accuracy requirements are specified in the MISR Data System Science Requirements [M-5] (DSSR) and will be summarized here for completeness.

The first product requirement is for imagery in each spectral band of the MISR nadir camera to be geolocated to ±250 m in both the cross-track and along-track directions for radiances projected to the smooth surface of reference ellipsoid WGS84, and ±275 m for radiances projected to the surface terrain (including topographic relief effects). These are specified at a confidence level of 95%. The geolocation requirement insures accurate placement of MISR data products on a geographical grid and co-registration of MISR imagery of a particular target acquired on multiple orbits, thereby insuring the ability to separate actual temporal changes on the Earth from misregistration errors.

The second product requirement is for imagery of a particular target from all bands of the nine MISR cameras to be spatially co-registered with an uncertainty of ±250 m cross-track and ±500 m along-track at a confidence level of 95%, for the ellipsoid-projected radiances; these values become ±275 m cross-track and ±550 m along-track for the surface projections. Registration of the data at these levels is driven primarily by the aerosol and surface retrievals, but is also necessary for the TOA/cloud retrievals in order to provide input of high geometric fidelity into the retrievals.

2.2 GEOMETRIC PROCESSING SCENARIO

The essential objective of the algorithms underlying MISR geometric processing is to assure

accurate georectification of the MISR image data. This georectification represent geometric transformations of 36 spectral bands of image data, so they all conform to a common map projection. For that purpose, algorithms used must address the following issues:

a) Definition of MISR pixel's pointing directions during imaging sequence, throughout the mission. This include removal of the errors embodied in navigation and attitude data, and in some of the parameters which define pointing directions internal to the instrument.
b) Removal of the distortions introduced by surface topography while imaging with the significantly different viewing angles.
c) Resampling of the acquired image pixels values in order to determine values to be assigned to the map projection grid.

In addition, the algorithm used must take into account the design of the processing system which satisfies the following criteria:

d) Balance between limited hardware resources, huge data volume and processing requirements.
e) Autonomous and non-stop production of the final product (i.e.,Georectified Radiance Product).

The scenario adapted for MISR geometric processing recognizes three major algorithms:

1) **Preflight geometric calibration algorithm:** This algorithm focuses on the initial definition of the Camera Geometric Model (CGM). The CGM is a mathematical expression that gives an arbitrary pixel's viewing direction, relative to the instrument coordinate system, as a function of several variables. The input to this algorithm is obtained through the preflight geometric calibration measurements conducted on the ground. The output from this algorithm (i.e., parameters defining the CGM) is used as one input to the in-flight geometric calibration algorithm. A more detailed description of this algorithm is given in the document "MISR Preflight Calibration Plan (JPL D-11392)".
2) **In-flight geometric calibration algorithm:** This algorithm consists of two parts: Part one focuses on the removal of the distortions introduced to the CGM created on the ground. These distortions are results of the deformations of the mechanical connections between the cameras, optical bench and the spacecraft platform, caused by launch and gravity release of the camera system. Part two focuses on the production of the specific information useful for the routine removal of the navigation and attitude errors, and distortions due to the surface topography. This information is stored in the Projection Parameters (PP) and Reference Orbit Imagery (ROI) files which along with the CGM construct the Geometric Calibration Dataset (GCD) to be used as the input to the L1B2 standard processing algorithm. The algorithm theoretical basis underlying production of the GCD is the subject of this document.
3) **L1B2 standard processing algorithm:** This algorithm focuses on the utilization of the supplied navigation and attitude data in conjunction with the provided GCD in order to produce required Georectified Radiance Product. The design of the algorithm reflects the autonomous and

continuous characteristics of the production, as well as the data volumes and processing capabilities of the production hardware. The detail description of this algorithm is given in MISR reference document [M-10].

2.3 GEOMETRIC CALIBRATION ALGORITHM OVERVIEW

2.3.1 Objectives

One of the unique challenges of MISR L1B2 data processing subsystem is to routinely and autonomously georectifiy and coregister imagery from 36 spectral bands with widely varying view angles. However, routine L1B2 processing (described in the L1B2 ATB document) rely on the GCD as the input. So, a geometric calibration effort must be completed in order to expect that georectification and coregistration accuracy requirements are continuously satisfied during standard processing.

The calibration process is divided into two segments. The first segment, Camera Geometric Model Calibration, focuses on the calibration of the camera physical and derived parameters which are used to define a pixel's pointing direction relative to the EOS AM-1 spacecraft reference point. The second segment, called Creation of the Projection Parameters and Reference Orbit Imagery, focuses on the correction of errors embodied in the navigation data (EOS AM-1 ephemeris and attitude) which are used to define position and pointing of the spacecraft relative to the Geocentric Inertial Coordinate System (GCI).

The Camera Geometric Model Calibration will be conducted preflight (i.e., in the MISR calibration laboratory) and in-flight, during the first few months after launch. During the mission, in-flight camera calibration will be repeated occasionally, in particular: 1) at a selected date, once a year, 2) after lunar maneuver, 3) after a report from the EOS Operation Center which indicate possible changes of MISR pointing, and 4) after standard processing performance indicators, resulting from the validation, suggest possible deviation from the previously calibrated CGM. In the case of a lunar maneuver happening once a year, 1) and 2) may be combined into one instance. The preflight measurements, described in the [14], will not include effects of the launch and gravity release deformations of the mechanical connections between the optical bench and the satellite platform, etc. Therefore, the objective of the In-flight Camera Geometric Model Calibration is to recalibrate parameters of the camera which are significantly sensitive to those effects.

The Creation of the Projection Parameters and Reference Orbit Imagery will generate input for the L1B2 standard processing with three major objectives: 1) to provide routine elimination of the errors in the navigation data, 2) to provide routine elimination of the topographic effects on the georectified imagery, and 3) to significantly simplify the standard processing algorithm and reduce its processing load.

The final result of the overall geometric calibration is the Geometric Calibration Dataset which consists of the calibrated Camera Geometric Model (CGM), the Projection Parameters (PP), and the Reference Orbit Imagery (ROI). This dataset is needed for successful L1B2 standard process-

ing.

2.3.2 Algorithm Outline

In order to present the concepts behind the MISR Geometric Calibration algorithm, two ways of viewing the algorithm will be introduced. The first view is with respect to time, resulting in two processes called: 1) Preflight Geometric Calibration, and 2) In-flight Geometric Calibration. The division with respect to the objectives of calibration, results in two parts called: 1) Camera Geometric Model (CGM) Calibration, and 2) Creation of Projection Parameters and Reference Orbit Imagery. However, these two views intersect each other. An illustration of the breakdown of the calibration algorithm is given in Table 1. This table does not include preparation of the ancillary dataset (e.g., ground control points). That kind of work is included in the calibration development activities and is separate from the calibration algorithm.

Table 1: Geometric Calibration Algorithm Breakdown

OBJECTIVES / *TIME*	Characterize Elements of Camera Geometric Model (e.g., boresight angle)	**1)**Elimination of the errors in navigation data. **2)** Elimination of topographic effects **3)**Simplification of standard L1B2 processing
Before Launch	PREFLIGHT CAMERA GEOMETRIC MODEL CALIBRATION	N/A
After Launch	IN-FLIGHT CAMERA GEOMETRIC MODEL CALIBRATION	CREATION OF PP AND ROI

It should be pointed out that the completion of the Creation of PP and ROI depends on the completion of the In-flight CGM calibration. However, a number of tasks can be completed simultaneously. An overview of the individual tasks is given in the following sections.

2.3.3 Preflight Camera Geometric Model Calibration

The MISR preflight calibration activity includes a group of measurements which are called preflight camera geometric model calibration. The camera model is a mathematical expression that gives an arbitrary pixel's viewing direction, in an appropriate coordinate system, as a function of several variables (the camera model is explained in more detail, in §3.3.2. The objectives of the preflight camera geometric model calibration is to characterize those variables (i.e., parameters) in order to: 1) verify that instrument science requirements (geometric) are satisfied before launch, and 2) provide input to the in-flight geometric calibration. The various parameters require different types of calibration, given their sensitivities and expected changes during the life of the instrument. Some of the parameters can be measured simply by inspection or set at specified values during assembly. Other parameters, particularly those sensitive to temperature changes, require more complicated calibration approaches.

For example, the effective focal length will depend on a number of variables, one of those being temperature. The Code V model of lenses will be used to predict distortion of effective focal length (see [15]). The prediction of Code V will be verified during the preflight field-of-view test. This test is also called "pixel-θ measurement", and is used to determine the focal length as a function of the temperature and field position. If the test results agree with the model we will be able to reliably predict in-flight focal length based on the temperature telemetry. The test will be done in the MISR thermal vacuum chamber (optical characterization chamber (OCC), and is the responsibility of the optical engineering team. More about this test can be found in [9].

The other challenging preflight calibration task is to define the orientation of a given camera to the optical bench. The measurements of these parameters is the primary motivation behind development of the Collimator Array Tool (CAT) which is described in [22]. The objectives of the CAT measurements are: 1) to verify that camera pointing angles are within the required tolerances of their nominal values, 2) to determine the degree to which pointing varies with temperature, 3) to determine if pointing varies in a repeatable fashion with temperature and verify related requirements, and 4) to verify pointing stability requirements. The CAT boresight algorithm, which will translate CAT measurements into the camera boresight error, is described in a number of design file memoranda (see [13] and [14]).

Current plans are to pursue an extensive calibration phase for the MISR instrument immediately after the protoflight cameras are built. In addition, the camera pointing will be verified at several points in time between instrument assembly and launch.

2.3.4 In-flight Geometric Calibration

2.3.4.1 Introduction

Due to the deformations of the mechanical connections between the optical bench and the spacecraft platform, caused by launch and gravity release on the camera system, certain parameters of

the camera model must be recalibrated during flight. The In-flight Camera Geometric Model calibration is designed to accomplish this task. In addition, a goal of the in-flight geometric calibration is to provide the means to remove, automatically, the effects of navigation errors and surface topography on the Georectified Radiance Product during standard processing using a simplified approach. The In-flight creation of the Projection Parameters (PP) and Reference Orbit Imagery (ROI) is designed to accomplish these goals.

Since the creation of the PP and ROI will deal with the geometric errors of the complete system, including the spacecraft, MISR optical bench, and individual MISR cameras, the in-flight CGM calibration will focus on each of the cameras independently. The output of the in-flight CGM calibration is required as an input to the creation of the PP and ROI.

2.3.4.2 In-flight Camera Geometric Model (CGM) Calibration

.

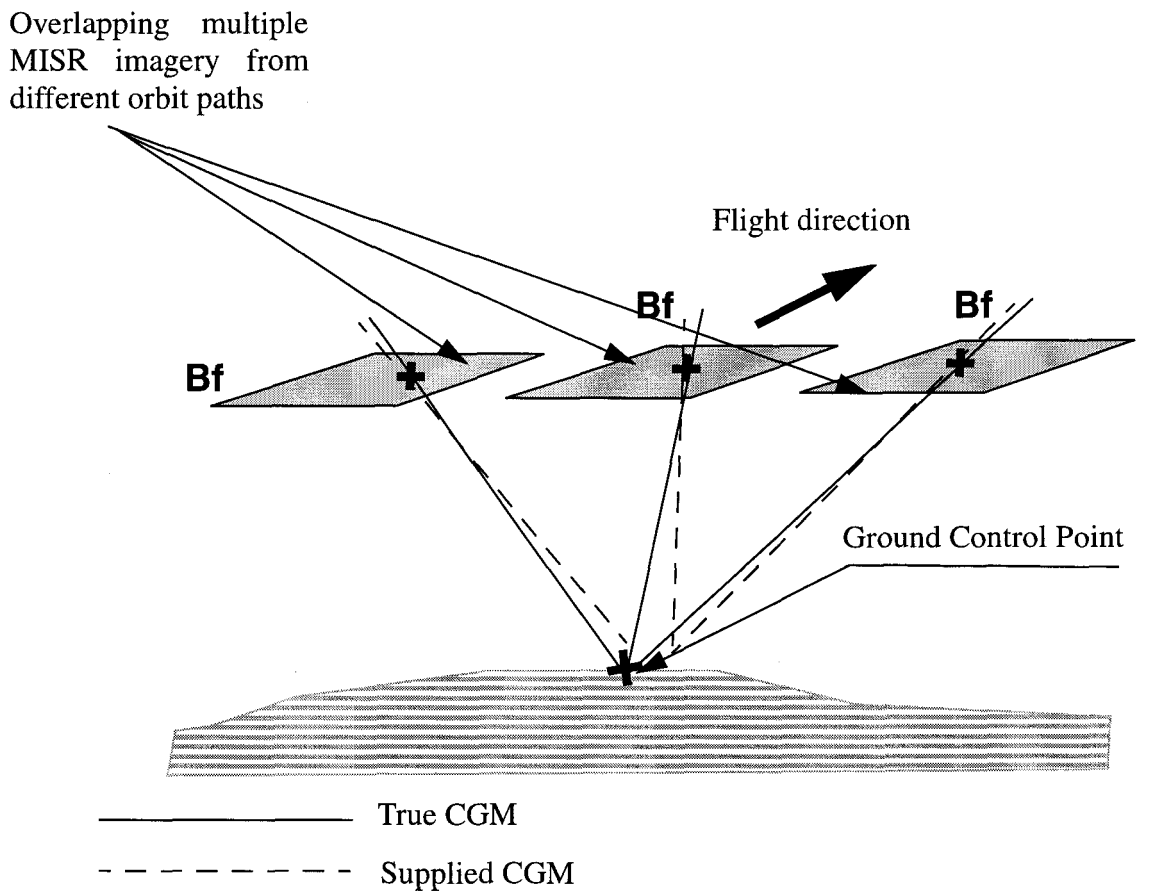

Figure 1: In-flight CGM Calibration

Some of the parameters of the camera model previously characterized during preflight calibration must be verified on orbit. The exact set of parameters to be recalibrated is given in Table 2. The recalibrated values must stay inside a priory assigned range. Otherwise, in-flight calibration data and procedures must be reexamined by the members of the Georectification Algorithm Team (see "In-flight Geometric Calibration Plan" JPL D-13228. page 4-6). In the case of findings detrimental to the overall quality of georectified product, the higher management level (i.e., Principal Investigator and Science Data System Manager) have to be informed. The calibration algorithm will make use of Ground Control Points (GCPs) and it will focus on the recalibration of each camera individually. The idea is to isolate static and systematic (e.g., temperature dependent) errors of the individual cameras from the errors reported in the navigation data. This is possible by having a large number of observations by a single camera of well-defined and well-distributed ground targets or GCPs.

A mathematical expression used to describe the ray between a ground point and the image of that point, as seen by a MISR camera, is used as the model for the least-squares estimation of certain camera model parameters. A large number of observations and good distributions of GCPs is needed so that effects of the errors in the navigation data on the estimation of the camera model parameters can be fully minimized. In that regard, it should be pointed out that a single GCP will be seen multiple times from a single camera during a 16-day period. This is important because it significantly increases the number of observations and, at the same time, provides a good distribution of ground control points across a camera field of view.

2.3.4.3 In-flight creation of Projection Parameters (PP) and Reference Orbit Imagery (ROI)

The Level 1B2 Georectified Radiance product must satisfy the geometric science requirements as stated in the Data System Science Requirements (DSSR) document. The calibrated Camera Geometric Model, even in the case when it meets the geometric instrument science requirements, may not be sufficient to provide a georectified radiance product of the desired accuracy. After applying the calibrated camera model, two types of errors remain significant: 1) errors in the navigation data, and 2) displacements due to the surface topography. The following approach is adopted and will be conducted at the SCF in order to remove the effects of those errors. The final result are PP and ROI files.

A) Adjustment.
A "simultaneous bundle adjustment" (a least square data estimation technique) constrained by a relatively high resolution Digital Elevation Model (DEM) is used to improve the accuracy of the navigation data later used to produce ROI to correspond to PP generated using nominal navigation data.

The "simultaneous bundle adjustment" takes advantage of the following MISR characteristics: 1) at a single instant of time MISR "sees" nine different, widely separated, targets on the ground, and 2) a single location on the ground is seen at nine different instants of time. If the

errors in the navigation data are modeled as time dependent then it is possible to write a mathematical model which will utilize known MISR characteristics and improve the accuracy of the navigation data.

This model is certainly good for improving relative accuracy (during a time period) of the navigation data. In order to obtain absolute accuracy (i.e., relative to a fixed ground coordinate system) additional ground control information is needed. For that purpose, in addition to already available GCPs, a high resolution DEM can be included as a good constraint to the adjustment.

Also, an algorithm which will accurately identify conjugate (e.g., tie, common) points in the nine images is used as a supplement to the bundle adjustment. This algorithm uses feature extraction and feature matching techniques in order to do identification of conjugate points without human intervention. A supporting method with a human operator in the loop, will also be in place. This interactive method will be used mostly for validation purpose and some infrequent occasions where improvement of the automatic detection of tie points is needed.

B) Forward Projection (Projection Parameters).
Using the nominal navigation data, the displacements of the ground points seen by MISR cameras due to the surface topography combined with MISR cameras viewing angle are computed. These displacements are computed using a high accuracy (i.e., subpixeling) forward projection method. Important additional information given by this method is that ground points obscured from MISR cameras are recorded. The results of this computation are called projection parameters and they are stored in a file which will be delivered to the DAAC.

C) Reference Orbit Imagery.
The operations described in A will be done a limited number of times while the operation described in B will be done only once at the beginning of mission. The generated PP will provide data which are effectively free of the errors in the navigation data and errors due to the topography. In order to take advantage of such information during standard processing, imagery corresponding to the PP must be created. This imagery is called Reference Orbit Imagery (ROI) and is used during image matching of continuously incoming imagery. The creation of the ROI involves a type of image resampling and mosaicking in order to conform PP and to obtain maximum cloud-free regions.

2.4 SUPPORTING DATA SETS

The methods proposed for the in-flight geometric calibration require certain data sets to be prepared and tested before launch. The purpose of these data sets is to either provide initial pointing of MISR cameras or to provide additional ground (non-spacecraft) information so that pointing can be improved. The three separate data sets are:

1) Camera Geometric Model dataset (preflight)

This dataset is the result of the preflight camera geometric calibration. It consists of a set of parameters which are used to define the pointing direction of an arbitrary pixel, in the instrument (i.e., optical bench) coordinate system. These parameters reflect distortions (including temperature dependencies) from the ideal optical system. Some of these parameters will be recalibrated in-flight.

2) Ground Control Points (GCPs)

A single ground control point is a geolocated image patch of a well-defined and easily identifiable ground feature. This ground feature must be found and precisely located in the MISR image, primary via an automated image matching technique or by visual stereo measurement as the second choice. The optimum size (e.g., about 30x30 MISR pixels) of the image patch is driven by the image matching algorithm requirement. The image patch must be produced from the digital imagery with ground resolution much higher than that of MISR. In addition, a corresponding DEM with the appropriate accuracy is needed in order to produce an image patch which is adequate with respect to the geometry and sampling characteristics of MISR cameras.

Ground control points are used to detect errors in the pointing of a MISR camera, at two occasions during in-flight calibration. First, they are used in order to separate navigation errors from the errors in the camera geometric model, so that parameters of this model can be updated. Later, ground control points will be used as an excellent constraint while correcting for navigation data errors. In both cases, the geolocation accuracy, number, and distribution of the GCPs is very important. For example, a pole to pole distribution of GCPs is needed in order to remove errors in temperature dependent camera parameters. Also, GCPs should be uniformly distributed across the FOV of a single camera. While searching for and preparing GCP image chips the goal is to obtain accuracy of 1/10 of a MISR nadir pixel for the ground location of the features representing the GCP. More accurate GCPs would not be useful since the 1/10 of a pixel is the accuracy limit of the image matching algorithm. However, depending on the nature and the size of the errors in the camera model somewhat less accurate (no worse than 1/2 of a pixel) GCPs will still be useful during calibration. An optimum required number and distribution of the GCPs will be established during calibration development time. The current estimate is 40 points. However, the calibration software will not be limited to a fixed number of GCPs.

3) Digital Elevation Model (DEM)

A global digital elevation map will be prepared from DMA DTED-1 data. Gaps in the existing DTED-1 land coverage will be filled with other sources of DEM data (i.e., DCW, ETOP-5). This global elevation map is also called DTED Intermediate Dataset (DID), and it will be prepared for MISR by the Cartographic Application Group (CAG) at JPL. The DID is basically a single DEM dataset consisting of multiple subgrids (physical files), where each subgrid is divided into many identically formatted tiles using the TIFF-6 file format. The elevation postings are on a 3 arcsec grid regardless of the original data source. However, information necessary to determine the source of each posting, elevation accuracy, and possible artifacts will be a part of the DID.

The DID is used to: a) compute effects of the topography on the geometry of the images taken from nine different viewing angles, and b) as the ground control surface (not point) information used while detecting errors in the navigation data.

2.5 GEOMETRIC CALIBRATION DATASET (GCD)

The final product of in-flight geometric calibration is the Geometric Calibration Dataset (GCD) which will be delivered to the DAAC, and used as input to L1B2 standard processing. The GCD consists of two major parts:

1) **Camera Geometric Model dataset:** This dataset consists of a set of parameters which are used in a mathematical expression in order to define the pointing direction of an arbitrary pixel. The viewing vector directions are relative to the spacecraft coordinate system. These parameters reflect geometries of the camera system and account for distortions (including temperature dependencies) from the ideal optical system. In particular there will be nine sets of parameters corresponding to the nine MISR cameras.
   The CGM approach is a fairly common way of defining the pointing direction of an individual pixel relative to the appropriate coordinate system. It has been used in a number of remote sensing mapping missions. Of course, the number and type of parameters depend on the individual sensor characteristics. If translated to the photogrammetric terminology the CGM may be called "interior orientation parameters". Using the same language, the supplied navigation data will define what are called "exterior orientation parameters". Thus, the CGM in conjunction with the supplied navigation data will provide the pointing vector of an arbitrary pixel, relative to the Earth-fixed (i.e., Conventional Terrestrial Reference) coordinate system. This pointing vector is the fundamental information, relative to the geolocation issues, used during L1B2 standard processing, for both the terrain-projected and ellipsoid-projected radiance product (see MISR reference document [M-10]).
2) **Projection Parameters (PP) and Reference Orbit Imagery (ROI):** The final result of the L1B2 standard processing is MISR imagery orthorectified (i.e., corrected for terrain displacement) and projected to the Space Oblique Mercator (SOM) map grid, which is also used to define Projection Parameters files. The separation between grid points is 275 m which is the nominal ground spacing of the pixels in the MISR images. The ground location of a grid point is given by the definition of the SOM map. The image location of a grid point is given by the pair of coordinates, called the projection parameters. A set of projection parameters covering the SOM map grid as seen by a single camera and corresponding to the red band image data is called the Projection Parameters file. There will be nine PP files for each of 233 MISR orbit paths. A specific MISR image related to the PP file is called Reference Orbit Imagery (see Figure 2). Even though the PP file and ROI correspond to a single orbit path the ROI will be created from several different orbit passes in order to minimize cloud cover. Both of these files, in addition to the pairs of coordinates (PP) and radiance value (ROI), will have some flag data in order to identify conditions like cloudy-clear, or land-ocean, for example.

   The PP and ROI are used as supplement to the projection vectors obtained from the CGM and

supplied navigation data, when producing terrain-projected radiance product. In particular, the PP is used to establish an intersection of that pointing vector with the terrain other than a water body at sea level; ROI is used via image matching with the new imagery to provide the pointing correction needed due to the errors in the supplied navigation data. For the ellipsoid-projected radiances, pointing corrections obtained through the image matching are extrapolated so they can be applied to the mathematically defined ellipsoid surface. Similarly, in the areas like large deserts and cloud covered regions use of ROI is not attainable so that geolocation and coregistration accuracy is limited by the accuracy of the calibrated CGM, supplied navigation data, and the extrapolated pointing corrections.

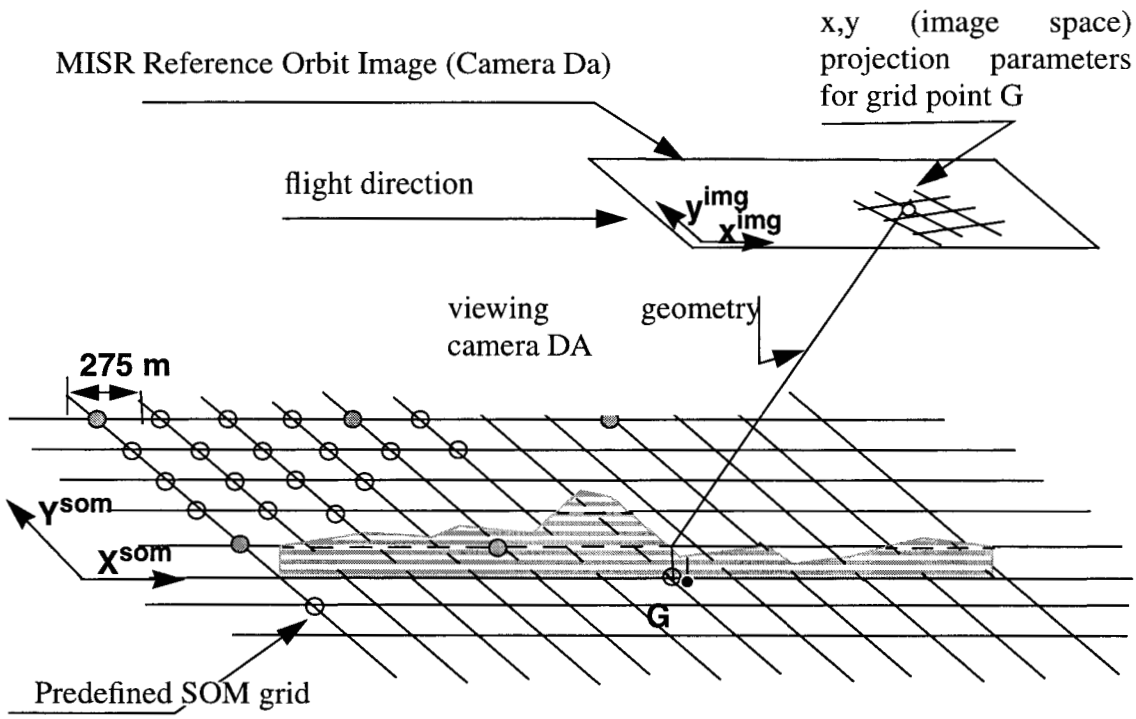

Figure 2: Projection Parameters and Reference Orbit Imagery

2.5.1 Geometric Calibration Dataset as input to L1B2

2.5.1.1 Introduction

The L1B2 standard processing algorithm and the Geometric Calibration Dataset were designed concurrently in order to make the standard processing algorithm more robust and less computationaly intensive. In particular, PP and ROI data concepts were created due to the specific MISR

geometric characteristics and demanding L1B2 standard processing requirements. Having PP and ROI as input will make the routine and autonomous nature of the L1B2 processing much more feasible. In order to have the standard processing working before in-flight calibration is completed, a crude GCD will be initially delivered to the DAAC. During this time the L1B2 standard product will be produced but the geolocation and coregistration accuracy will directly depend on the preflight camera calibration and supplied navigation data only.

2.5.1.2 Use of the calibrated Camera Geometric Model

The CGM approach is a fairly common way of defining the pointing direction of an individual pixel relative to the instrument coordinate system. It has been used in a number of remote sensing mapping missions. Of course, the number and type of parameters depend on the individual sensor characteristics. If translated to photogrammetric terminology the CGM consist of "interior orientation parameters". Using the same language, the supplied navigation data will define what is called "exterior orientation parameters". So, CGM in conjuction with the supplied navigation data will provide the pointing vector of an arbitrary pixel, relative to the Earth fixed (i.e., Conventional Terrestrial Reference) coordinate system. This pointing vector is the fundamental information, relative to the geolocation issues, used during L1B2 standard processing, for both the terrain-projected and ellipsoid-projected radiance product (see MISR reference document [M-10]).

2.5.1.3 Use of the PP and ROI

The PP and ROI are used as a supplement to the projection vector obtained from the CGM and supplied navigation data, while producing the terrain-projected radiance product. In particular, the PP is used to establish an intersection of that pointing vector with the terrain other than a water body; ROI is used via image matching with the new imagery, to provide the pointing correction needed due to the errors in the supplied navigation data. For the ellipsoid-projected radiance product pointing corrections obtained through the image matching are extrapolated so they can be applied to the mathematically defined ellipsoid surface. Similarly, in areas like large deserts and cloud covered regions, use of ROI is not attainable so that geolocation and coregistration accuracy is limited by the accuracy of the calibrated CGM, supplied navigation data, and the extrapolated pointing corrections.

3.0 ALGORITHM DESCRIPTION

3.1 INTRODUCTION

The focus of this section is on the mathematical aspects of the in-flight geometric calibration algorithm. The algorithm is divided input, processing and output parts which are further decomposed into smaller entities which are then mathematically described. The goal of this section is to provide a theoretical description of the algorithm.

3.2 PROCESSING OUTLINE

The algorithm starts with the in-flight calibration of the Camera Geometric Model. Once this part is finished creation of the Projection Parameters and Reference Orbit Imagery can begin. A pictorial description is given in Figure 3.

The calibration of the CGM first involves identification of Ground Control Points and their precise measurement in image space. This is accomplished via an area-based image matching method. After that a least-square resection method is used to estimate certain parameters of the CGM. This process is done on a camera by camera basis using certain number of previously prepared GCPs.

The creation of the PP and ROI starts with the nominal orbit navigation and attitude data. In particular, the nominal PP file is created at the beginning of mission along with the ROI which is empty at this point. Later, once imagery is acquired a correction of its supplied navigation and attitude will be obtained in order to accurately relate this imagery to the nominal PP during mosaicking process. The identification of tie (i.e conjugate) points between nine (or less) MISR cameras is required as the input for the corrections of navigation data. Most of the GCPs can be used as the tie points. This is accomplished through a combination of feature extraction, feature matching, and area-based image matching. The next step is simultaneous bundle adjustment where corrections to the supplied navigation data are estimated. The last step is the production and assembly of the Reference Orbit Imagery which involves image mosaicking.

3.3 ALGORITHM INPUT

3.3.1 Introduction

The algorithm input data can be divided into two groups. The first group represents input data which will be calibrated and those are: (a) Camera Geometric Model, and (b) Spacecraft Navigation and Attitude data. The second group represent data which will provide ground control information useful for calibration and those are: (a) Ground Control Points, and (b) DTED Intermediate Dataset (DID). This subsection provides a mathematical formulation and use of the

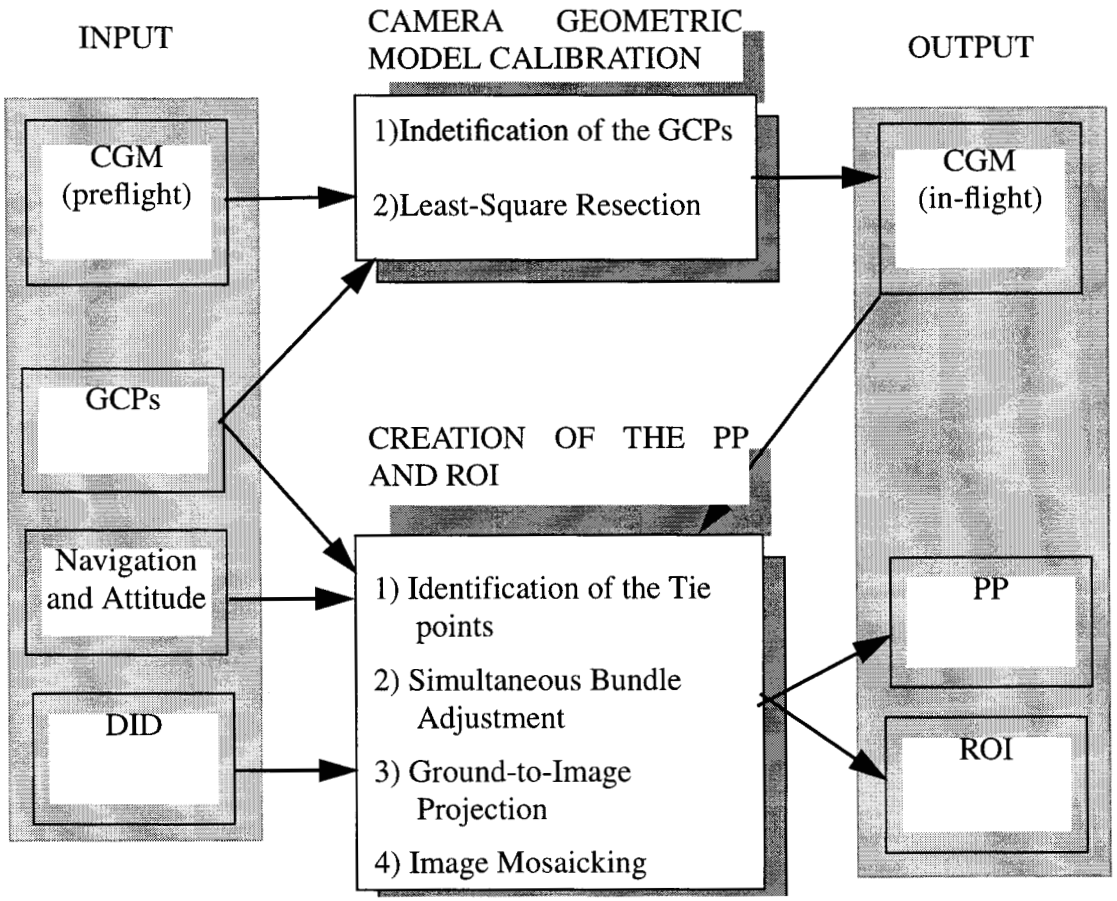

Figure 3: In-flight Calibration Algorithm Processing Outline

input data.

3.3.2 Camera Geometric Model (CGM)

The CGM (created preflight) is the set of parameters and the mathematical expression relating to those parameters for defining the viewing vectors of the ground points where image coordinates are measured. The viewing vector directions are relative to the spacecraft coordinate system. Following are descriptions of the various transformation which translate image coordinates to the vector in the spacecraft coordinate system. The information presented here is based on the interoffice memo [15]. The complete definitions of the coordinate systems introduced in this section are given in Appendix A. The Table 2 gives sample of the CGM parameters for red bands of few cameras as measured for $5°C$ temperature.

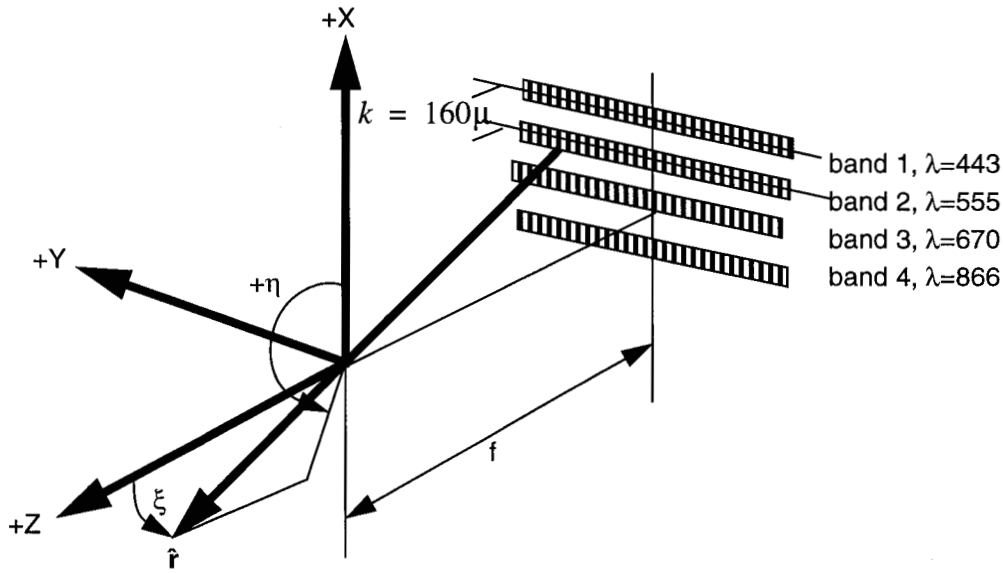

Figure 4: Detector Coordinate System of the Camera Geometric Model

Transformations

1) Image plane - focal plane.

Let's say that l, s are image line and sample coordinates in the band $n (n = 1, 2, 3, 4)$. The line coordinate increases along the spacecraft track and the sample coordinate increases in the West - East direction across the track from, thus forming a right hand coordinate system with the line axis. The image coordinates need to be adjusted prior to converting it to focal plane coordinate system. The adjustment of the line coordinate is required due to the push-broom nature of MISR camera where every line has its own projection center and can be treated as the individual frame. Therefore adjusted image line coordinate l' represent only fractional part of measured line location and its always range from –0.5 of the detector size to + 0.5 of the detector size with 0.0 corresponding to the center of a image line. The appropriate line adjustment equation is $l' = (l - INT(l + 0.5))d_x$, where d_x represent detector pitch in x direction and INT stands for the integer part of a floating-point number. The sample adjustment is necessary due to the number of covered detectors in the line array and reverse readout order for some of the cameras. The adjusted sample coordinates s' can be computed as $s' = s + sc + 1$ in the case of direct readout (i.e. detector 1 is on the West side of image) or $s' = st + sc - s$ in the case of reverse readout order (i.e. detector 1 is on the East side of image). The sc is the number of covered detectors on the beginning of the CCD line array while st is equal total number of active pixels in the CCD line array. The focal plane coordinates x_f, y_f at temperature T, as the function of adjusted image coordinates are:

$$x_f = k(n, T) + l'$$
$$y_f = f(n, T) \cdot \sum_{i=0}^{5} \alpha_i(n, T) \cdot s'^i \quad (1)$$

In equation (1) the CGM parameters used are:

$k(n, T)$ - downtrack angle of band n at temperature T between boresight pixel and X-Z plane of the detector coordinate system. As the sign convention, positive angle corresponds to the location of the band on the positive side of detector coordinate system.

$f(n, T)$ - effective focal length for band n at temperature T.
$a_i(n, T)$ $i = 0, 1, 2, 3, 4, 5$ pixel-theta coefficients for band n at temperature T.These coefficients account for the distortions of the field angle in the cross-track direction. The exact set of distortion coefficients for all lens types is measured in the Optical Characterization Chamber. The above described set of camera parameters is measured at three temperatures, 0, 5, and 10 degrees Celsius, in order to verify that there is not significant changes in the parameters for this temperature range. During the flight temperature will be controlled to stay at 5 degree Celsius.

2) Focal plane - Detector Coordinate System

The unit vector of the viewing direction in the Detector coordinate system is:

$$\hat{r}_{dcs} = \mu \begin{bmatrix} -x_f \\ -y_f PT \\ f \end{bmatrix} \quad (2)$$

where: $\mu = (x_f^2 + y_f^2 + f^2)^{-1/2}$, and f is the effective focal length. The PT is the flag related to the direction of the measured pixel-theta coefficients. Normally it is equal 1. However, there is potential of misunderstanding this direction while analyzing calibration report. In that case PT flag in the camera geometric dataset would be set to -1 avoiding any change in the software.

3) Detector Coordinate System - Camera Coordinate System

The unit vector of the viewing direction in the Camera Coordinate System is:

$$\hat{r}_{ccs} = \begin{bmatrix} B0 & 0 & 0 \\ 0 & B0 & 0 \\ 0 & 0 & 1 \end{bmatrix} \begin{bmatrix} \cos\varepsilon & -\sin\varepsilon & 0 \\ \sin\varepsilon & \cos\varepsilon & 0 \\ 0 & 0 & 1 \end{bmatrix} \begin{bmatrix} \cos\psi & 0 & \sin\psi \\ 0 & 1 & 0 \\ -\sin\psi & 0 & \cos\psi \end{bmatrix} \begin{bmatrix} 1 & 0 & 0 \\ 0 & \cos\theta & -\sin\theta \\ 0 & \sin\theta & \cos\theta \end{bmatrix} r_{dcs} \quad (3)$$

Table 2: Camera Geometric Model Parameters - sample for red band at $5°C$

Cam.	Readout PT BO	Boresight	Downtrack angle $k(3, 5)$ deg	Det. pitch d_x, d_y (mm)	f_0 (mm)	$\alpha(a_0, \ldots)$	ε (deg.)	ψ, θ (deg.)	$\delta;\beta$ (deg.)	$\omega_z, \omega_y, \omega_x$ (deg.)
Df	reverse 1 1	750.7	-0.065	0.018; 0.021	123.67	1.2747e-01 . .	-0.2759	0.0; 0.0	-28030 58.1266	0.006666 -0.041111 -0.0658333
An	direct 1 -1	764.82	-0.050	0.018; 0.021	58.944	2.71992e-01	-0.1518	0.0; 0.0	0.0022 0.0016	0.006666 -0.041111 -0.0658333
Da	direct 1 -1	762.0	-0.0358	0.018; 0.021	123.653	1.2941e-01	0.0691	0.0; 0.0	2.7314 -579879	0.006666 -0.041111 -0.0658333
Calibration										
Pre-flight	defined	measured in OCC at three tempera-tures	measured in OCC at three temperatures	measured by inspection	measured in OCC at three temperatures	measured in OCC	measured by CAT	measured in OCC	measured by CAT	N/A
In-flight	verified	no	no	no	yes	no	no	no	yes	yes
Sensitivity		gravity release (max. 0.2 pix.)	none	none	thermal	thermal	none	none	thermal & gravity release	thermal and gravity release

where CGM parameters are:

ε, ψ, θ - small angle vector rotations around Z, Y, and X axes of the Detector Coordinate System, which are used to form transformation matrix T_{cd}. As the sign convention, the positive angle is a counter clockwise rotation of the vector when looking at the origin from the positive end of the axis. The flag BO is equal 1 in the case of direct band orientation (i.e. detector and camera closely oriented in the same direction) or -1 in the case of inverse band orientation.

4) Camera Coordinate System - Instrument Coordinate System

The unit vector of the viewing direction in the Instrument Coordinate System is:

$$\hat{r}_{ics} = \begin{bmatrix} \cos\beta & \sin\beta\sin\delta & \sin\beta\cos\delta \\ 0 & \cos\delta & -\sin\delta \\ -\sin\beta & \cos\beta\sin\delta & \cos\beta\cos\delta \end{bmatrix} \hat{r}_{ccs} \tag{4}$$

where the CGM parameters are:

δ - rotation around the X axis of the Instrument Coordinate System.

β - rotation around Y axis of the Instrument Coordinate System.

The β and δ form transformation matrix T_{ic}

5) Instrument Coordinate System - Spacecraft Coordinate System

The unit vector of the viewing direction in the Spacecraft Coordinate System is:

$$\hat{r}_{scs} = \begin{bmatrix} \cos\omega_z & \sin\omega_z & 0 \\ -\sin\omega_z & \cos\omega_z & 0 \\ 0 & 0 & 1 \end{bmatrix} \begin{bmatrix} \cos\omega_y & 0 & -\sin\omega_y \\ 0 & 1 & 0 \\ \sin\omega_y & 0 & \cos\omega_y \end{bmatrix} \begin{bmatrix} 1 & 0 & 0 \\ 0 & \cos\omega'_x & \sin\omega'_x \\ 0 & -\sin\omega'_x & \cos\omega'_x \end{bmatrix} \hat{r}_{ics} \tag{5}$$

where the CGM parameters are:

ω_z, ω_y, ω_x - small-angle rotations representing a non-sequential misalignment between ICS and SCS, which form transformation matrix T_{si}. As the sign convention, positive angle is counter-clockwise rotation of the instrument coordinate system axis towards the spacecraft coordinate axis when looking at the origin from the positive end of rotation axis. Since the angles are a non-sequential combination the ω'_x is derived to be $\omega'_x = \text{asin}((\sin\omega_x)/(\cos\omega_y))$

All of the parameters listed are separately measured throughout preflight calibration. Once the instrument is mounted on the spacecraft and launched into the orbit, effects of the certain parameters (i.e., angles β, δ, and ω) can not be measured explicitly. Instead, a resulting total effect will

be measured and assigned only to the selected parameters. So, the in-flight calibrated CGM may not facilitate the best characterization of the individual physical parameters of the camera, but it will provide the most accurate total pointing vector.

3.3.3 Spacecraft Navigation and Attitude Dataset

In order to relate a vector referenced to the spacecraft coordinate system (e.g., $\hat{r}_{scs}$) to the ground coordinate system, the spacecraft navigation and attitude data must be known.

The navigation data of special interest to the in-flight geometric calibration are spacecraft position and velocity vectors. The navigation system uses a high accuracy output based on the TDRSS Onboard Navigation System (TONS) as the primary method of producing navigation data. The second (backup) means of navigation is a coarse accuracy output based on propagating a set of uplinked Brouwer-Lyddane mean orbit elements. In the spacecraft "Normal Mode" primary and backup navigation operate in parallel in order to facilitate the execution of fault detection, isolation, and recovery logic. The TONS navigation filter provides near real-time estimates of EOS-AM position and velocity every 10.24 seconds. The Guidance, Navigation and Control Subsystem (GN&CS), which provides position and velocity every 1.024 seconds, uses a second order Taylor series integrator to do estimation between TONS measurements. The position and velocity vectors are reported relative to the Geocentric Inertial Coordinate System of the mean Equator and Equinox of J2000. They are used to define the relation between the Orbital Coordinate System and the Geocentric Coordinate System at an instant of time. If $\hat{P}$ is position and $\hat{V}$ is velocity then the transformation between these two coordinate system can be written as:

$$T_{go} = \left[\hat{x}\ \hat{y}\ \hat{z}\right] \tag{6}$$

where

$$\begin{aligned} \hat{z} &= -\frac{\hat{P}}{\|\hat{P}\|} \\ \hat{y} &= \frac{\hat{z}\times\hat{V}}{\|\hat{z}\times\hat{V}\|} \\ \hat{x} &= \hat{y}\times\hat{z} \end{aligned} \tag{7}$$

The attitude data are produced through an attitude determination algorithm based on Kalman filtering theory. This algorithm receives measurements of stars or Sun and provides a 6-element state correction vector consisting of 3 small angle attitude errors and 3 gyro bias compensation errors. Calls are made to the Kalman update filter every 10 seconds, if stellar or solar measurements are available. At other times the attitude is propagated using gyros. The GN&CS provides attitude angles relative to the Orbital Coordinate System, and attitude rates relative to the Spacecraft Coordinate System every 1.024 seconds. The attitude angles, i.e., roll Ω, pitch Ψ, and yaw

K, are used to define the transformation between the two coordinate systems:

$$T_{os} = \begin{bmatrix} \cos\Psi\cos K & \sin\Omega\sin\Psi\cos K - \cos\Omega\sin K & \cos\Omega\sin\Psi\cos K + \sin\Omega\cos K \\ \cos\Psi\sin K & \sin\Omega\sin\psi\sin K + \cos\Omega\cos K & \cos\Omega\sin\Psi\sin K - \sin\Omega\cos K \\ -\sin\Psi & \sin\Omega\cos\Psi & \cos\Omega\cos\Psi \end{bmatrix} \quad (8)$$

Combining (6) and (8) with (5) the viewing direction expressed in the Geocentric Inertial Coordinate System is:

$$r_{gci} = T_{go} T_{os} r_{scs} \quad (9)$$

To summarize, the spacecraft navigation and attitude dataset is provided by GN&CS through the spacecraft ancillary data message. It consist of: a) spacecraft position and velocity vectors relative to the Geocentric Inertial Coordinate System, and b) attitude angles (i.e., roll, pitch and yaw) relative to the Orbital Coordinate System, and attitude rates expressed in the Spacecraft Coordinate System.

For calibration purposes, access to the spacecraft ancillary data message can be made in two ways: 1) through the internal MISR Engineering Navigation dataset created by the MISR instrument, or 2) through PGS toolkit calls made at the SCF, assuming that required files are staged at the SCF. Idea is to normally use second method having MISR Engineering Navigation dataset as a backup.

The TONS accuracy estimates and attitude determination accuracy estimates fall well within the three-sigma navigation and attitude knowledge requirements. However, one of the goals of the in-flight calibration is to remove unexpected and significant errors embodied in this data. For that purpose additional terms will be added to the model (9) and that topic is the subject of §3.4.2.3 (Simultaneous Bundle Adjustment).

3.3.3.1 Nominal Spacecraft Navigation and Attitude Dataset

A number of MISR ancillary dataset will be produced prior to launch. Two of those: 1) Ancillary Geographic Product (AGP), and 2) Projection Parameters (PP) file depends on the spacecraft navigation and attitude dataset. In order to save time and simplify processing we decided to use nominal spacecraft ephemeris as specified prior to launch. Also, we will set nominal attitude angles to be zero.

The simulated nominal spacecraft ephemeris are produced using a Kepler orbit mode approximation l. As the simplified orbit model, without J2 and drag term, Kepler model can not be used for a longer time period. However, this orbit approximation is fine for a single path. So we divide simulation of spacecraft ephemeris into 233 segments forcing the ephemeris to correspond to 233 orbit path as defined for the EOS-AM1 spacecraft. These 233 orbit paths are defined as the equator

crossings and are called World Reference System (WRS). It should be pointed out that same WRS will be used for Landsat 7 spacecraft. Orbit elements used for ephemeris generation are Brouwer Mean True-of-Date elements as specified in Table 2:

Table 2: Orbit Elements

Orbit Element	Latest estimate
Epoch	1998-06-30T00:00:00
Semi-major axis	7078040.8 meter
Eccentricity	0.00116241
Inclination	98.30382 degrees
Argument of perigee	90.004875 degrees
Right ascension of descending node for path 1	295.4000 degree
Mean Anomaly at epoch	25.57689 degrees
Orbit Period	5932.8 seconds
WRS orbit path at epoch	93

3.3.4 Ground Control Points (GCP)

Ground Control Points will be used as the most accurate and valuable information against which the CGM is calibrated and corrections to the navigation data are computed. Each GCP consists of an image chip which contains a well defined and easily indefinable ground feature. The shape of the image chip should preferably be a square. The size of one side of the square should be somewhere between 16 and 30 MISR pixels. The image chip must be produced from source imagery with much higher resolution than MISR (e.g., 30 m) together with the associated DEM so that the GCP image chip can be warped for the specific MISR viewing geometry and still provide accurate ground location. The image of a single ground point will be used to produce 9 image chips for the nine MISR cameras. The software called MISRSIM will be used to produce these warped image chips form the accurately registered images and DEMs. Seasonally invariant features (e.g., man-made objects, coastlines) are the first choice for GCPs. Otherwise, more than one image source corresponding to a single GCP should be used, in order to reflect seasonal variations.

A very important characteristic of the GCP is the accurate geo-location of the center of the image chip. This ground location is expressed through the X_{ctr}, Y_{ctr}, and Z_{ctr} coordinates relative to the Conventional Terrestrial Reference Coordinate System (i.e., Earth fixed). Since the direction between spacecraft center of mass (within ±3 m) and GCP is the same as the image viewing direction to that GCP, if both are expressed relative to the Geocentric System, GCP is used to

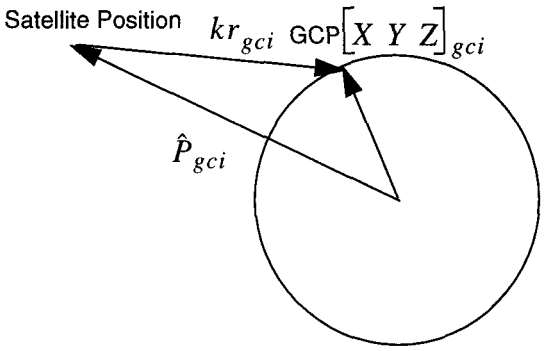

Figure 5: GCP in relation to the camera vector

complement model (9) in the following way:

$$T_{gc}\begin{bmatrix} X_{ctr} \\ Y_{ctr} \\ Z_{ctr} \end{bmatrix} = \hat{P}_{gci} + kr_{gci} \tag{10}$$

where T_{gc} is the transformation between Conventional Terrestrial Reference and Geocentric Inertial coordinate systems at the instant of time when the GCP is observed. The coefficient k is a scale factor.

It should be pointed out that for the imaging event with oblique viewing angles and sensor high above the ground atmospheric refraction effects must be taken into consideration. In particular, the ray leaving the instrument (i.e., defined as r_{gci} in (10)) slightly change its direction as it goes through the atmosphere towards the ground. It has been shown that for the MISR imaging geometry a standard refraction offset based on the standard atmospheric condition is adequate correction. As a matter of fact, this correction is significant only for the two most oblique D cameras. The standard offsets computed in will be taken into account by adjusting the vector r_{gci}.

3.3.5 DTED Intermediate Dataset (DID)

The DID is a seamless global Digital Elevation Map (DEM) compiled from DMA DTED-1 and other non-DMA data. In order to access these data special "DID retrieval" software is required. The DID and the "DID retrieval" software are produced by the Cartographic Application Group (CAG) at JPL.

The user of the DID may specify size and location of the geographical grid with 3 arcsec spacing and obtain the following information on each of the 3 arcsec postings: 1) elevations in meters, relative to the Mean Sea Level, 2) flags indicating "land", "water", or "boundary" types of surface, and 3) meta-DEM data indicating source of the DEM postings and quality (accuracy) identifier.

During in-flight geometric calibration DID will be used to determine an equation of the surface over a small (max 6 x 6) rectangle. Such an equation of the surface is used as the constraint while modeling errors in the navigation and attitude data.

Initially, using only supplied navigation and attitude the ground location of the image point of interest will be determined. Then a rectangular grid of limited size of the elevation postings surrounding the ground point can be extracted from the DID. Using latitude, longitude (lat_i, lon_j, where $i, j = 0, 1, \ldots N$ is the size of the grid) and elevations (h_{ij}) a general function of the continues interpolated surface of the form

$$h = P(lat, lon) \tag{11}$$

can be determined where P may belong to the family of either bilinear, biquadratic, or bicubic interpolating functions. During simultaneous bundle adjustment (subsection §3.4.2.3) the least-square estimate of the ground coordinates (X_{ctr}, Y_{ctr}, Z_{ctr}), is made while removing errors from the navigation and attitude data. These ground coordinates will be additionally constrained with equation (11) if they are related to the lat, lon, and h as follows

$$\begin{aligned} X_{ctr} &= (N+h)\cos(lat)\cos(lon) \\ Y_{ctr} &= (N+h)\cos(lat)\sin(lon) \\ Z_{ctr} &= (N(1-e^2)+h)\sin(lat) \end{aligned} \tag{12}$$

These equations (12) represent the transformation between Geodetic and Geocentric coordinate systems, where N is the ellipsoid radius of curvature in the prime vertical, and e is the ellipsoid eccentricity.

Without surface constraints (i.e., Equations (12) used in simultaneous bundle adjustment) modeling of the navigation and attitude errors will be limited to the relative effects only (utilizing multi-viewing capability of MISR). However, in order to account for absolute error, the surface equation is the second best constraint after the GCPs, which in some cases can be scattered too far from each other.

3.4 THEORETICAL DESCRIPTION

3.4.1 In-flight Camera Geometric Model Calibration

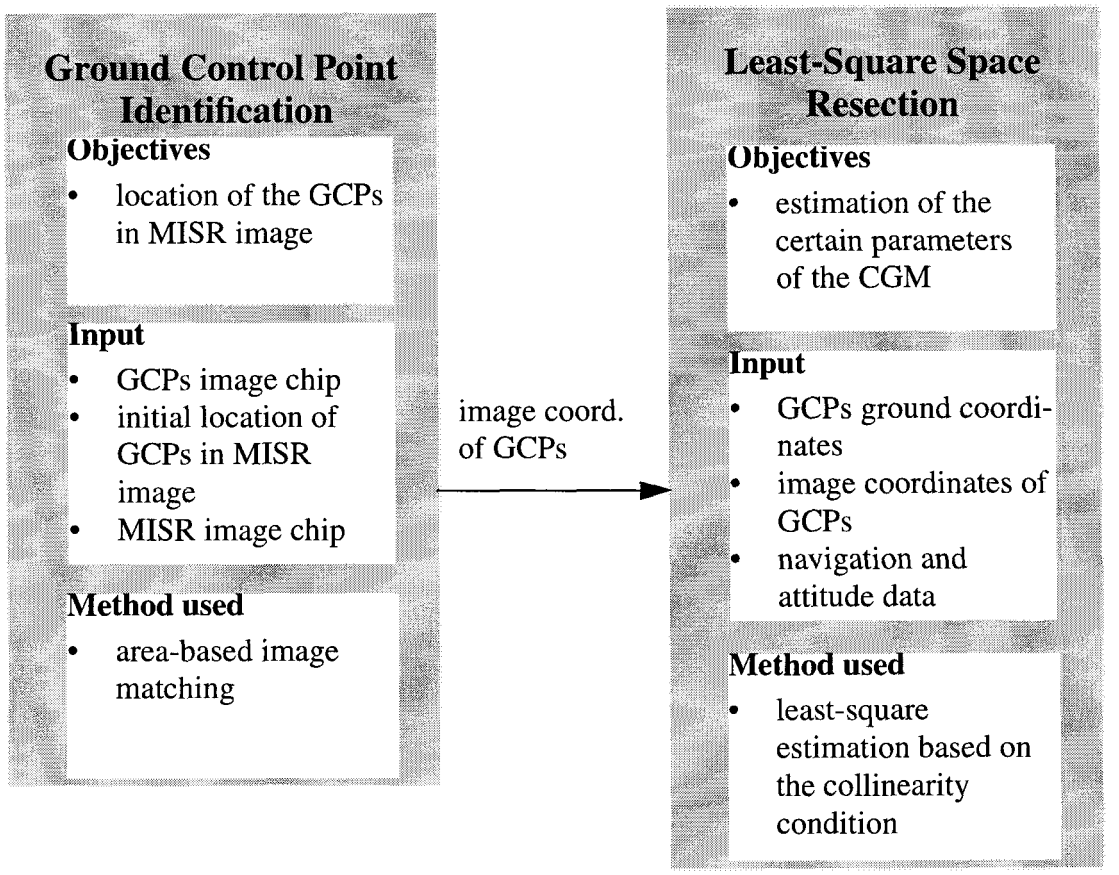

Figure 6: Outline of the In-flight Camera Geometric Model Calibration

3.4.1.1 Introduction

The objective of this part of the in-flight geometric calibration is to recalibrate some of the elements of th CGM. In this part of the calibration no attempt will be made to model navigation and attitude data errors. Instead, a statistical removal of these errors will be made through the use of well defined and accurate GCPs and a large number of observation of these GCPs. This calibration task consist of two parts: a) Identification and measurement of the location of the GCP in MISR image and b) Least-square estimation of certain parameters of the CGM, so called least-square resection.

3.4.1.2 Ground Control Point Identification

Objective

The objective of this part is precise image location of a GCP defined by the image chip and ground coordinates of the center of that image chip. The image matching technique is a combination of the cross-correlation and least-square area-based methods. It is suggested theoretically, and supported empirically, that the geometric uncertainty of the least-square matching can be as low as ± 0.05 of the pixel. The accuracy of the match depends mainly on the signal-to-noise ratio and on the image texture. Consequently, good image texture is one of the requirements on the image chips used for GCPs.

The identification of a single point using GCPs is independent from the identification of others, and is the same for all of the GCPs. The discussion here is limited to the measurement of a single point in the single camera.

Input

1. The GCP image chip I_{gcp} of size $N \times N$.

2. MISR image chip I_{misr} of size $M \times M$. The center of I_{misr} is located at line, sample l_{ii}, s_{ii} coordinates of MISR images. The l_{ii}, s_{ii}, initial locations of the GCP, are computed from the supplied navigation and attitude data using Image Point Intersection (IPI) function (see reference document [M-10]). The amount by which M exceeds N reflects the extent of the combined errors in the CGM, and navigation and attitude data.

Mathematical Description

First, a cross-correlation algorithm is implemented as follows: The image chip I_{gcp} is shifted over the larger I_{misr} in a pixel-by-pixel steps. At each of the steps, or pixels, located at $(l_{ii} + \Delta l, s_{ii} + \Delta s)$ in the larger image a similarity measure is obtained. Specifically, using gray level values of the surrounding overlapping pixels, a variation of the normalized cross-correlation is computed as follows:

$$C_{(l_{ii} + \Delta l, s_{ii} + \Delta s)} = \frac{\sigma_{misr,gcp} \cdot |\sigma_{misr,gcp}|}{\sigma^2_{misr} \cdot \sigma^2_{gcp}} \tag{13}$$

where $\sigma_{misr,gcp}$ is the covariance between MISR and GCP image chips, and σ^2_{misr},σ^2_{gcp} are the variances. The $\Delta l, \Delta s$, offsets from the center of I_{misr}, change in increments of 1 pixel in the

interval $\pm(M-N)/2$. The locations $l_i = l_{ii} + \Delta l$ and $s_i = s_{ii} + \Delta s$ are where the cross-correlation is at maximum (indication of the match with the GCP) and are new centers of the I_{misr} chip that are now used as the input to the least-square matching.

In the least-square matching the geometric and radiometric transformations between two image chips are estimated by minimizing certain functions between them. Let:

x',y' be the coordinates in the I_{gcp} relative to the rectangular coordinate system with the origin set at the center of that image chip.

x'',y'' be the coordinates in the I_{misr} relative to the rectangular coordinate system with the origin set at the point l_i,s_i.

Then the geometric relation is modeled by the affine transformation

$$\begin{aligned} x'' &= F_x(x', y') = a_0 + a_1 \cdot x' + a_2 \cdot y' \\ y'' &= F_y(x', y') = a_3 + a_4 \cdot x' + a_5 \cdot y' \end{aligned} \tag{14}$$

Also, if

$$\begin{aligned} g' &= G'(x', y)' + n'(x, y) \\ g'' &= G''(x'', y'') + n''(x'', y'') \end{aligned} \tag{15}$$

are the discrete radiance values for I_{gcp} and I_{misr} respectively, where G' and G'' are image functions, while n' and n'' are associated noise values, then the radiometric relation is expressed as a 2-parameter linear function:

$$g' = F_r(g'') = k_0 + k_1 \cdot g''(F_x, F_y) \tag{16}$$

To solve for the parameters a_i and k_j equation (16) needs to be linearized. This gives:

$$\Delta g + v = \sum_{i=0}^{5} k_1^{(0)} \cdot \left(g_x \cdot \frac{\partial F_x}{\partial a_i} + g_y \cdot \frac{\partial F_y}{\partial a_i} \right) \cdot da_i + \sum_{j=0}^{2} \frac{\partial F_r}{\partial k} \cdot dk_j \tag{17}$$

where $\Delta g = g'(x', y') - (k_0^{(0)} + k_1^{(0)} \cdot g''(x'', y''))$.

Before we start computing elements of the equation (16), a low pass filter of form

$$\begin{vmatrix} \frac{1}{10} & \frac{1}{10} & \frac{1}{10} \\ \frac{1}{10} & \frac{2}{10} & \frac{1}{10} \\ \frac{1}{10} & \frac{1}{10} & \frac{1}{10} \end{vmatrix} \tag{18}$$

is applied to both image chips in order to minimize noise, but without significantly degrading image texture. Image matching will be avoided in areas contaminated by pixels with an Image Data Quality Indicator (IDQI) that suggest radiometrically unusable data (IDQI are obtained through the L1B1 processing). Initially, and after each iteration, it is assumed that there are no more differences between the two image chips so parameters are set to be $(a_0, a_1, a_2, a_3, a_4, a_5, k_0, k_1)^0 = (0, 1, 0, 0, 0, 1, 0, 1)$. An iteration starts by computing the differences Δg from the gray level values of the corresponding pixels. The gradients g_x and g_y, in the x and y directions, are also estimated from the gray level values.

For each pair of the corresponding pixels in I_{gcp} and I_{misr}, one equation can be written. Then, the least-square technique is used to solve for the correction to the parameters of interest. The new set $(a_0, a_1, a_2, a_3, a_4, a_5, k_0, k_1)^m$ (m is the iteration number) is computed. Using this set I_{misr} is resampled (by means of bilinear interpolation) and radiometrically corrected. Also, locations l_i and s_i are updated as follows:

$$\begin{aligned} l_i^m &= l_i^{m-1} + a_0^m \\ s_i^m &= s_i^{m-1} + a_3^m \end{aligned} \tag{19}$$

Prior to the next iteration, parameters a_i and k_j are reset to their initial values. As can be seen, only two linear shifts are applied to the correction of the GCP location. This is due to the fact that this point is kept at the origin of the coordinate system in each of the iterations. The full set of geometric and radiometric parameters is used to resample I_{misr}. Iterations are terminated once the corrections to the parameters a_0 and a_3 are less than the assigned threshold (e.g., 0.01 of pixel). In the case when the estimated standard deviation of the least-square match does not get smaller of than preselected convergence criterion, the match is qualified as not possible.

Output

For a single GCP seen by one camera in a single orbit path, output from the GCP identification would be:

1. (l, s) : image coordinate of the GCP

2. $q = \begin{bmatrix} \sigma_l^2 & \sigma_{ls} \\ \sigma_{ls} & \sigma_s^2 \end{bmatrix}$: variance-covariance matrix of the estimated accuracy of GCP location.

It is most probable that a GCP would be identified in all nine cameras and in more than 1 orbit pass.

3.4.1.3 Least-Square Space Resection

Objective

Recalibration of certain parameters of the CGM is the objective of this part of in-flight geometric calibration.

The least-square resection of a single camera is independent from the other cameras, and is the same for all nine cameras.

Input

1. The GCP ground coordinates referenced to the Conventional Terrestrial Reference (CTR) Coordinate System: $G_j = \left[X_{ctr}\ Y_{ctr}\ T_{ctr}\right]_j$, where subscript j ($j = 1, 2, \ldots, n$) denote the jth GCP.

2. Output from the GCP identification process, image coordinates (ICs) of the GCPs and associated variance-covariance matrix: $IC_{j,i} = \left[l\ s\ q\right]_{j,i}$ where subscript i ($i = 1, 2, \ldots, m$)denote the ith orbit pass over the jth GCP.

3. The navigation and attitude data (NA) associated with the time when a GCP is observed: $NA_{j,i} = \left[P_x\ P_y\ P_z\ V_x\ V_y\ V_z\ \Omega\ \Psi\ K\right]_{j,i}$. Note that the NA dataset is extracted (based on the $l_{j,i}$ coordinate) from the spacecraft ancillary data (see section §3.3.3).

Mathematical Description

Looking back on Figure 5, the statement can be made that the camera, GCP and image of that point all must lie on the same line. The mathematical form which expresses this geometric condition is termed the collinearity condition. The final form, which is going to be used in this least-

square estimation, can be derived from the equation (10). Let us say that $G_{gci} = T_{gc} \times \left[X_{ctr}\ Y_{ctr}\ Z_{ctr}\right]^T$ is the GCP vector in the Geocentric Inertial frame. Then (10) can be rearranged as:

$$k \cdot r_{gci} = G_{gci} - P_{gci} \tag{20}$$

The vector r_{gci} is derived (sections §3.3.2 and §3.3.3), to be:

$$r_{gci} = \mu \cdot T_{go} T_{os} T_{si} T_{ic} T_{cd} r_{dcs} \tag{21}$$

In order to further rearrange (20), the transformation from the Geocentric Inertial to the Detector coordinate system is set to be $M = [T_{go} T_{os} T_{si} T_{ic} T_{cd}]^T$, so that

$$r_{dcs} = \frac{1}{k\mu} \cdot M \times [G_{gci} - P_{gci}] \tag{22}$$

or further (dropping out the subscripts which denote coordinate system)

$$\begin{bmatrix} -x_f \\ -y_f \\ f \end{bmatrix} = \frac{1}{k\mu} \cdot \begin{bmatrix} m_{11} & m_{12} & m_{13} \\ m_{21} & m_{22} & m_{23} \\ m_{31} & m_{32} & m_{33} \end{bmatrix} \times \left[\begin{bmatrix} G_x \\ G_y \\ G_z \end{bmatrix} - \begin{bmatrix} P_x \\ P_y \\ P_z \end{bmatrix} \right] \tag{23}$$

Expanding the right hand side and dividing the first two equation by the third, leads to collinearity condition equations:

$$\begin{aligned} F_1(obs, par) &= x_f + f \cdot \frac{m_{11} \cdot (G_x - P_x) + m_{12} \cdot (G_y - P_y) + m_{13} \cdot (G_z - P_z)}{m_{31} \cdot (G_x - P_x) + m_{32} \cdot (G_y - P_y) + m_{33} \cdot (G_z - P_z)} = 0 \\ F_2(obs, par) &= y_f + f \cdot \frac{m_{21} \cdot (G_x - P_x) + m_{22} \cdot (G_y - P_y) + m_{23} \cdot (G_z - P_z)}{m_{31} \cdot (G_x - P_x) + m_{32} \cdot (G_y - P_y) + m_{33} \cdot (G_z - P_z)} = 0 \end{aligned} \tag{24}$$

which will be used as the mathematical model in the least-square resection. Since the equations (24) are non-linear the linearized form for a single ray (jth GCP seen on ith MISR image) would be:

$$a_{j,i} v_{j,i} + b_{j,i} \Delta = f^0_{j,i} \tag{25}$$

where a is a 2x2 matrix

$$a = \frac{\partial F}{\partial(observations)} = \begin{bmatrix} \frac{\partial F_1}{\partial x_f} \cdot \frac{\partial x_f}{\partial l} & \frac{\partial F_1}{\partial y_f} \cdot \frac{\partial y_f}{\partial s} \\ \frac{\partial F_2}{\partial x_f} \cdot \frac{\partial x_f}{\partial l} & \frac{\partial F_2}{\partial y_f} \cdot \frac{\partial y_f}{\partial s} \end{bmatrix} \tag{26}$$

v is a 2x1 vector of observational residuals. If we assume that β, δ and ε are the parameters of the CGM which are going to be recalibrated, then b is a 2x3 matrix

$$b = \frac{\partial F}{\partial(parameters)} = \begin{bmatrix} \frac{\partial F_1}{\partial M} \cdot \frac{\partial M}{\partial \beta} & \frac{\partial F_1}{\partial M} \cdot \frac{\partial M}{\partial \delta} & \frac{\partial F_1}{\partial M} \cdot \frac{\partial M}{\partial \varepsilon} \\ \frac{\partial F_2}{\partial M} \cdot \frac{\partial M}{\partial \beta} & \frac{\partial F_2}{\partial M} \cdot \frac{\partial M}{\partial \delta} & \frac{\partial F_2}{\partial M} \cdot \frac{\partial M}{\partial \varepsilon} \end{bmatrix} \tag{27}$$

and Δ is a 3x1 vector of parameter corrections. f^0 is a pair of functions evaluated at the actual observations and initial values (pre-flight CGM) of the parameters of interest.

For n GCPs seen in m MISR images (25) can be written as:

$$\begin{bmatrix} a_{1,1} & 0 & \dots & 0 & \dots & 0 \\ 0 & a_{1,2} & \dots & 0 & \dots & 0 \\ \dots & \dots & \dots & 0 & \dots & 0 \\ 0 & 0 & 0 & a_{1,m} & \dots & 0 \\ \dots & \dots & \dots & \dots & \dots & 0 \\ 0 & 0 & 0 & 0 & 0 & a_{n,m} \end{bmatrix} \times \begin{bmatrix} v_{1,1} \\ v_{1,2} \\ \dots \\ v_{1,m} \\ \dots \\ v \end{bmatrix} + \begin{bmatrix} b_{1,1} \\ b_{1,2} \\ \dots \\ b_{1,m} \\ \dots \\ b_{n,m} \end{bmatrix} \times \Delta = \begin{bmatrix} f^0_{1,1} \\ f^0_{1,2} \\ \dots \\ f^0_{1,m} \\ \dots \\ f^0_{n,m} \end{bmatrix} \tag{28}$$

or in more compact form

$$AV + B\Delta = F^0 \tag{29}$$

If the matrix

$$Q = \begin{bmatrix} q_{1,1} & 0 & \dots & 0 & \dots & 0 \\ 0 & q_{1,2} & \dots & 0 & \dots & 0 \\ \dots & \dots & \dots & 0 & \dots & 0 \\ 0 & 0 & 0 & q_{1,m} & \dots & 0 \\ \dots & \dots & \dots & \dots & \dots & 0 \\ 0 & 0 & 0 & 0 & 0 & q_{n,m} \end{bmatrix} \tag{30}$$

is the variance-covariance matrix of the line and sample observations for the GCPs, then the least-square solution of the system of equations (29) and (30) for the corrections of the vector Δ is given in [19].

$$\Delta = [B^T(AQA^T)^{-1}B]^{-1}[B^T(AQA^T)^{-1}F^0] \tag{31}$$

or in more compact form

$$\Delta = N^{-1}T \tag{32}$$

Given the specific structure of the matrix A, Q, B and F^0 the matrix N^{-1} (3x3 matrix) can be evaluated as

$$N^{-1} = \left(\sum_{j=1}^{n} \sum_{i=1}^{m} b_{j,i}^T (a_{j,i} q_{j,i} a_{j,i}^T)^{-1} b_{j,i} \right)^{-1} \tag{33}$$

and matrix T (3x1 matrix) is

$$T = \left(\sum_{j=1}^{n} \sum_{i=1}^{m} b_{j,i}^T (a_{j,i} q_{j,i} a_{j,i}^T)^{-1} f_{j,i}^0 \right) \tag{34}$$

The least-square solution is iterative, and since the initial values of the parameters would be close to their real value (results of pre-flight calibration), the convergence would be of second order and relatively fast. The criteria for termination of iterations is based on the fact that parameter correction should approach zero.

Output

The output from the Least-Square Resection would be the entire same set of CGM parameters, with the selected subset of those parameters recalibrated using the GCP.

3.4.2 Creation of PP and ROI

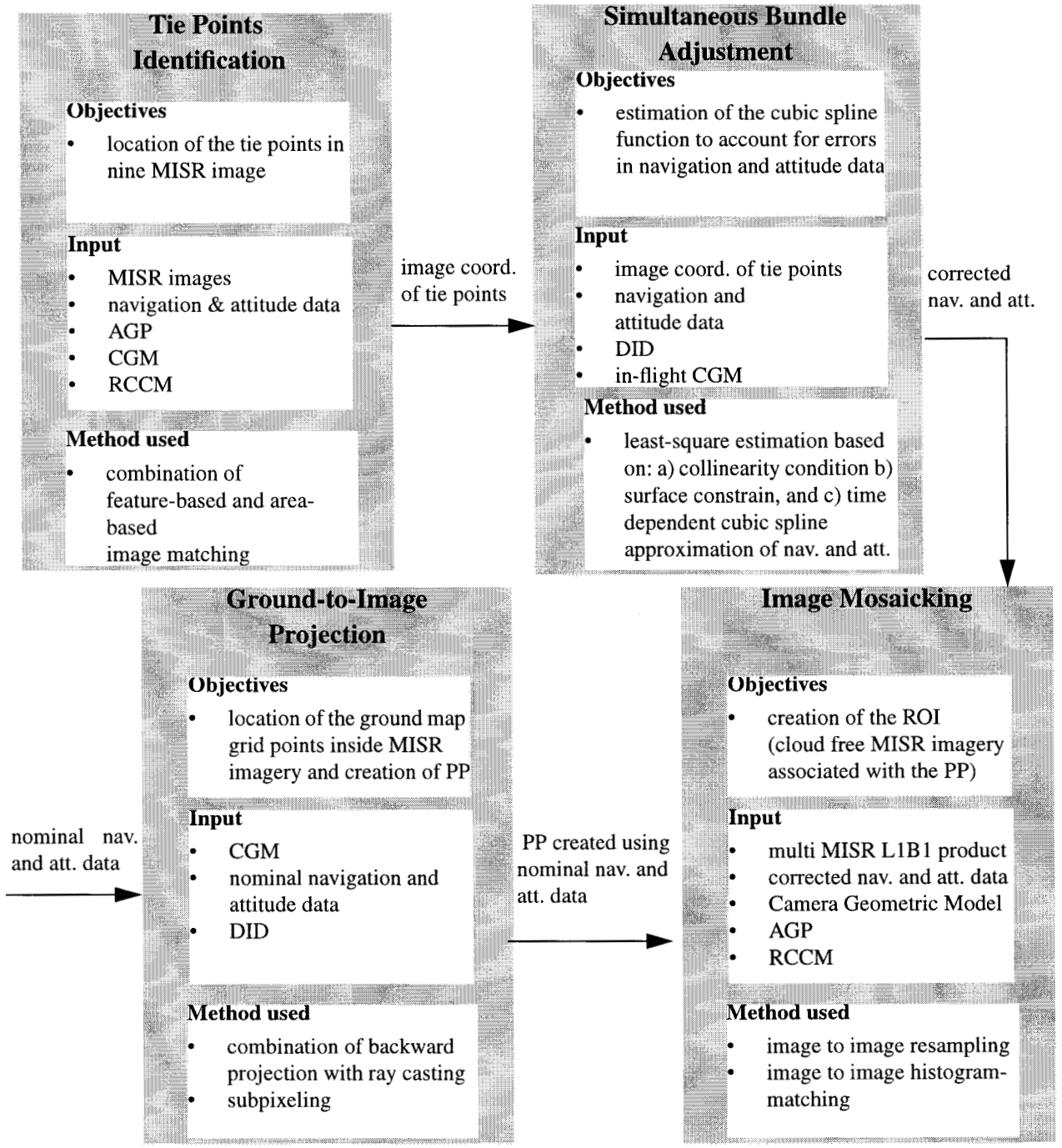

Figure 7: Outline of the processing for the creation of PP and ROI

3.4.2.1 Introduction

The EOS-AM platform will make a total of 233 revolutions, or orbits per one repeat cycle which will last for 16 days. The creation of the ROI, in regards to these orbits primarily deals with the data on an orbit-by-orbit basis. Particularly, "Tie Points Identification" and "Simultaneous Bundle Adjustment" work with the data from all nine cameras corresponding to a single orbit at a time. The "Ground to Image Projection" which used the nominal orbit data works independently camera-by-camera. However, the mosaicking of the ROI may require data from several repeat revolutions of the same orbit path. As already mentioned there are four distinct parts of this segment of in-flight geometric calibration (see Figure 7)

3.4.2.2 Tie Points Identification

Objective

The overall objective of tie point (TP) identification is to produce a set of measured conjugate points which can be used as ties between MISR images obtained at the different instants of time. Conjugate points are the set of image points of the same ground point in the MISR images viewed by different cameras. The goal of this process is to first automatically extract distinct interest points in nine MISR images which have a high chance of being precisely identified in at least three MISR images, and second to match the extracted interest features over at least three MISR images. A set of well distributed, accurately and reliably identified tie points over a segment of MISR orbit are a major contribution to our ability to model errors in the navigation and attitude data.

The process of TP identification consists of four modules: building of an intermediate dataset called surface feature mask, initial matching of nine local conjugate image patches, feature-based matching of interest points, and precisely matching of final tie points.

Input

1. The images from all nine MISR cameras corresponding to one orbit path.

2. The supplied navigation and attitude data.

3. The AGP.

4. The RCCM.

Mathematical Description

Surface Feature Mask Creation

Surface features such as coast lines, ridges of mountains are usually presented as distinct features in the image space too. The essential of TP detection is to detect distinct image features from multiple images and match conjugate image point features. Therefore, the goal of creating surface feature mask (SFM) is to evaluate surface information and come up with a dataset which describes the potential of detecting image features in an area.

The evaluation of surface feature is conducted and reported at a resolution of 17.6 km region for the following reasons. First, in the following initial matching module, local conjugate image patches are to be extracted. The corresponding image size of 64 x 64 pixels to the 17.6 km surface region is adequately large to provide enough image overlap from camera to camera according to the navigation specification. Second, in the feature-based interest point matching, interest points are extracted and matched over the same image area of 64 x 64 pixels, which is also an adequate area for detecting a sufficient number of inter-related distinct interest point features for matching, as will be discussed later.

At each 17.6 km region, the following data are computed and collected into the SFM dataset based on 1.1 km AGP data:

1. Surface feature indicator:

   - *Coast line*: if the number of coast line pixels > T_c,
   - *Hill*: if the surface elevation standard deviation is larger than T_{min} and smaller than T_{max}.
   - *Water*: if the number of deep ocean, ocean or inland water pixel is larger than T_w,
   - *No distinct surface feature*: otherwise.

2. Surface elevation statistics:

   - *Elevation maximum*: h_{max},
   - *Elevation minimum*: h_{min},
   - *Elevation sdv*: σ_h.

3. The SOM x and y locations, and average regional elevation based on 1.1 km pixel average scene elevation within 17.6 km region.

The surface feature indicator will be used to determine the potential of detecting image features at each 17.6 km region. The three values of the surface elevation statistics will be used to determine the image search window and constraints the image matching process. The geolocation and elevation at the center of 17.6 km region will be used to determine the initial conjugate MISR image locations.

Initial Matching

The purpose of initial matching is to determine local conjugate image patches for all 9 MISR cameras on which precise TP identification can be conducted. In another word, initial matching reduces the image matching ambiguity and searching space. With the knowledge of orbit navigation and MISR attitude data, initial conjugate image locations can be determined for a given ground location using the image point intersection technique (IPI) with an accuracy of less than 10 pixels of error. This process is cheaper than most image matching techniques and is reliable. Around the initial conjugate image locations, the local conjugate image patches are extracted.

A surface region, at whose center we can apply IPI to locate 9 conjugate image patches, is called a tie point candidate (TPC). Generally, it is preferred that a TPC is located on an area with rich surface features. On the other hand, bundle adjustment requires a well-distributed TPs available in order to increase the adjustment accuracy and reliability. This requires detecting TPs in a regular space. Initial matching will therefore locate two types of TPCs on the surface space. The first type of TPC is called surface feature tie point candidate (STPC) and the second type is called grid tie point candidate (GTPC). Both STPC and GTPC are a surface region with size of 17.6 km.

A STPC is a surface region where the surface feature indicator in the SFM is either *coast line* or *ridge*. Due to the high potential of detecting TPs with high accuracy over a STPC, STPCs are determined at a relative dense resolution r_s (number of 17.6 km unit region). For example, we can search through the SFM data at a resolution of 3 x 3 of 17.6 km pixels, spirally detect STPC from the center pixel to neighboring ones by checking the surface feature indicators. A STPC is selected if any of these 9 pixels is either coast line or ridge. Hopefully we can select one STPC for each 3 x 3 window.

The purpose of GTPC is to provide a regular distribution of TP detection in case there are not enough STPC available in an area. A GTPC is determined within a grid defined according to a pre-defined resolution r_g (number of 17.6 km unit region). The grid resolution r_g is generally sparser than the STPC resolution r_s. It represents the optimal TP configuration required by bundle adjustment. A grid of resolution of r_g may not have a GTPC if there is already one or more STPC within the grid, or if every 17.6 km unit region within that grid is marked as *water* from SFM. A GTPC within a grid can be the first non featureless 17.6 km pixel found by a spiral search started from the grid center pixel. The spiral search is terminated if precisely matched TPs are detected on a selected TPC or all TPC within the grid have been selected. Figure 8 shows an example of selected TPCs where the shaded boxes are STPCs, the blank ones are GTPCs, and the dotted ones are selected TPCs without successfully detecting tie points over it.

It is desired that a TPC is a clear region seen from all 9 MISR cameras. It is possible that at both sides of the swath, image data for a particular camera is missing for a 17.6 km region. A valid local conjugate image patch is therefore defined as: 1) an image patch of size 64 x 64 image pixels centered at a conjugate image location determined by IPI; 2) all 64 x 64 image pixels are clear; 3) all 64 x 64 image pixels are within the MISR imagery boundary for the corresponding camera.

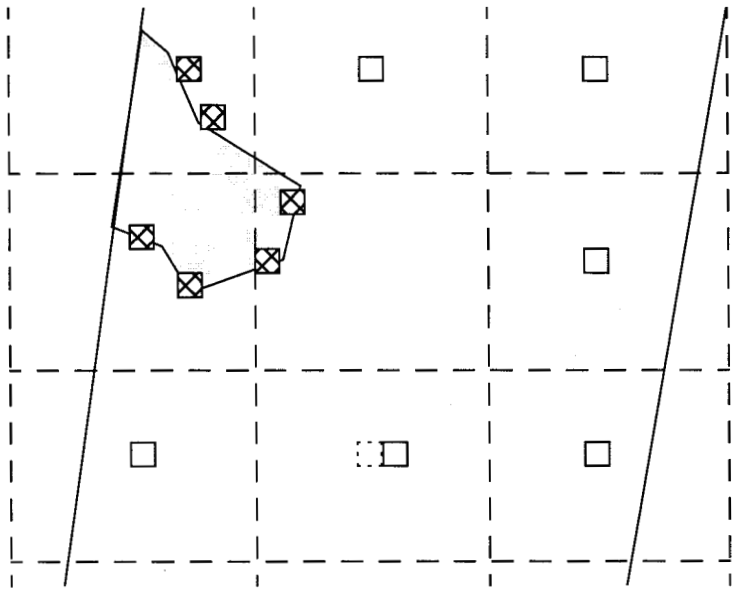

Figure 8: Tie-point candidates

The topographic projected Radiometric Camera-by-camera Cloud mask (RCCM) generated by L1B2 standard processing can be used to determine if an image patch is clear. RCCM is available at 1.1 km resolution. If all the 1.1 km pixels within an image patch for a camera is marked as clear with high confidence, the corresponding image patch is clear. Note that RCCM is determined with the knowledge of before-corrected navigation and attitude data. If there are at least minimum of 5 valid local conjugate image patches available for a 17.6 km region, this region is regarded to be a potential TPC. Otherwise, this region can not be a TPC.

Interest Point Feature Detection

The local conjugate image patches resulted from initial matching usually contain shifts and distortion from one image patch to another due to the errors in the navigation and attitude data, the imaging view angle differences, and the topographic variations. The goal of interest point (IP) feature detection is to find a robust IP operator and extract distinct image points features within the local conjugate image patches which are more likely to be invariant with respect to the expected geometric and radiometric distortions. Ultimately, the detected IPs are to be matched as our better guess of TPs over the initial matching, and to be served eventually as the prior knowledge of area-based matching.

A modified version of Forstner interest point (FIP) operator is employed for this application. The details about FIP operator is described in the reference paper [1]. In summary, FIP operator detects meaningful image point features such as intersection of line features (i.e. corner) or gravity centers of image gray level in a local window. It first computes the interest values of all image pixels by calculating the image gray value changes within a small window of size 3 x 3 or 5 x 5 centered at the pixel being evaluated. If dominant corner feature or gravity center of gray level is

presented in the evaluating window, the estimated error ellipsoid of image value variations will indicate it with high confidence. The optimal location of the interest point can be estimated in sub-pixel accuracy. Several modifications were made in our application of FIP operator. First, because of the non-uniform gray level distribution over satellite image data, FIP operator is applied locally. The detected "interest" points are only distinct relative to their local area instead of entire imagery across the swath. Selection of local conjugate image patches at a size about 64 x 64 pixels provides an adequate local area for the detection of interest points. The next modification to the FIP operator is that it is only applied on a set of basic interest points (BIP) instead of all image pixels. Therefore, the weight threshold is computed based only on the weight values of those BIPs instead of all image pixels. Such modification not only reduces the computation, but also increase the quality of the detection. The BIP operator is chosen to be the Robert IP operator, which can be referred to as reference [2]. The third modification to the use of FIP is the window size of the suppression of local non-maximum is set dynamically according to the number of BIP within the local conjugating image patch and the FIP weight. The purpose of this modification is to make the detection be more robust with respect to various global surface types that MISR image covers, and to various image qualities across different MISR cameras.

Although FIP operator is relatively expensive, it is more accurate and invariant comparing with most of other IP operators. This means that the detection of IP across of 9 MISR imageries viewed by camera from a large range of view angle are more likely to be conjugate ones than most other IP operators. This invariant property is very critical for the TP detection, especially while multiple image matching is required. IP detection results a list of IPs for each local conjugate image patch. Each IP has its line and sample coordinate in sub-pixel accuracy, and a weight indicates its interest value.

Interest Point Feature Matching

The matching of two lists of IPs from two conjugate images can be described as given a set of point features in one image, find the mapping of them with another set of point features in another image. This data mapping problem can be translated into a consistent labeling process.

Consistent labeling

According to [3], an N-ary *consistent-labeling problem* (CPL) is a 4 tuple CPL = (U, L, T, R). The first component U is a set of M units $U = \{1,...,M\}$, which are the objects to be labeled. The component L is the set of possible labels. The third component T is called the *unit-constraint relations*. T is an N-ary relation over the set U of units. Finally, R is called the *unit-label constrains*. R is an N-ary relation over the set U x L of unit-label pairs. If an N-tuple $[(u_1, l_1), (u_2, l_2), ..., (u_N, l_N)]$ belongs to R, then the unit, $u_1, u_2, ..., u_N$ may be assigned the corresponding labels $l_1, l_2, ..., l_N$. A labeling of a subset $\hat{U} = \{u_1, u_2, ..., u_N\}$ of U is a mapping f: $\hat{U} \rightarrow L$ from $\hat{U}$ to L. A labeling f of a subset $\hat{U}$ of units is consistent if whenever $u_1, u_2, ..., u_N$ are in $\hat{U}$ and the N-tuple $(u_1, u_2, ..., u_N)$ is in T, then $[(u_1, f(u_1)), (u_2, f(u_2)), ..., (u_N, f(u_N))]$ in R.

Now let A and B be two data sets. Let $T \subseteq A^N$ be an N-ary relation over set A. Let f: $A \rightarrow B$ be a function that maps elements of set A into set B. The *composition* of T with f is defined by:

$$T \circ f = \{(b_1, \ldots, b_N) \in B \mid \text{there exists } (a_1, \ldots, a_N) \in A \text{ with } f(a_i) = b_i, i = 1, \ldots, N\} \quad (35)$$

Let $S \subseteq B^N$ be a second N-ary relation. A *relational homomorphism* from T to S is a mapping f: $A \rightarrow B$ that satisfies $T \circ f \subseteq S$. A relational homomorphism maps the elements of A to a subset of the elements of B having all the same interrelationships that the original elements of A had. A r*elational monomorphism* is a relational homomorphism that is one-one. And finally, a *relational isomorphism* f from an N-ary relation T to an N-ary relation S is one-one relational homomorphism from T to S, and f^{-1} is a relational homomorphism from S to T. If we regard one data set A, such as a list of IPs, as a set of units and another data set B, such as another list of IPs from a conjugate image patch, as the set of labels. The unit-constraint relation is simply the relation T of the relational homomorphism problem. The unit-label relation R is given by R= $\{[(u_1, l_1), (u_2, l_2), \ldots, (u_N, l_N)] \mid (u_1, u_2, \ldots, u_N) \in T \text{ and } ((l_1, l_2, \ldots, l_N) \in S)\}$

Tree Search

To solve a consistent labeling problem, we look for the set of all consistent labeling f: $U \rightarrow L$ that satisfy the constraints specified by T and R. Assume there are M IPs from one local conjugate image patch, N IPs from another local conjugate image patch, and $M < N$. Choosing M set of IPs as the unit set, and N set of IPs as the label set, the labeling of the unit set to the label set constructs a problem space which can be represented by a tree with its depth equaling to M. Each node in the tree represents one labeling or pairing of a unit to a label. Each branch of the tree from the root to the leaf represents one of total

$$\sum_{i=1}^{M} \prod_{j=0}^{M-1} (N - j) \quad (36)$$

number of possible branches, only one of them is a consistent labeling or the correct matching. We hope to search for the consistent labelling and reject the in-consistent labelling efficiently. There are existing heuristic methods for pruning the tree. One of the basic concept of the heuristic approaching is to evaluate the cost for each pairing and always expands a the tree on a node with minimum cost. In the discipline of artificial intelligence, such an approach is called best-first search. The cost for one pairing is evaluated by an evaluation function, defined as:

$$f(n) = g(n) + h(n) \quad (37)$$

where $g(n)$ is the cost from the root of the tree to current node pairing, and $h(n)$ is the cost from the current pairing to the final leaf pairing. Note that we can only estimate the future cost as we

don't know that yet. In our application, the way that we estimate the cost of current pairing and future pairing is based on a future-error-table (FTAB). At each labeling, we evaluate not only the satisfaction of current constraints specified by T and R, but also the future consequences of the current labeling regarding to these constraints. Each element in the FTAB represents the error that deviates from labeling constraints. When this error is large enough, a labeling is considered to be impossible. We stop expanding the current branch and look backward for another node to expand. Therefore, the tree search method used in this application is rather a combination of the back-tracking and the best-first search. It is also called consistent labeling with forward checking.

Evaluation Function

Treat feature matching as consistent labeling, we must tolerant errors during the labeling because of the existence of the error in the IP detection and the image deformation from camera to camera. FTAB is then not a binary table, such as either possible or impossible, instead we set a threshold for FTAB. The following factors contributes to the errors in the FTAB:

1. Interest Value Similarity

The interest weight w of an IP describes the distinctness of an IP relative to its local surrand-ing.The conjugate IPs with a relative similar local image patterns tend to have similar interest val-ues according to the definition of FIP operator. The similarity of IPs can be measured by the relative difference between conjugate IPs, as defined as follows:

$$W_{sim} = \frac{w_l - w_u}{max\{min\{w_l, w_u\}, w_{min}\}} \tag{38}$$

where w is the IP weight for either unit or label, w_{min} is a pre-determined constant minimum interest value.

2. Radiometric Similarity

The relative radiometric similarity between a pair of IP from a pair of local conjugate image patches is defined as an unit-label constraint. This is done by opening an examining window of 5 x 5 centered at each of the matching IP pair. The similarity measurement is defined as:

$$R_{sim} = \frac{\sum_{w} fabs\{[img_l(r,c) - \overline{img_l}] - [img_u(r,c) - \overline{img_u}]\}}{\sigma_l}. \tag{39}$$

where $img(r, c)$ is the image value at the pixel location (r, c) from either the unit image patch, or the label image patch, $\overline{img}$ is the mean image value within the examining window, σ_l is the image value sigma within the label examining window. The summation is done within the exam-ining window. This is a relatively simple and cheap area-based similarity measurement and can be

computed for each pair of potential matching pairs.

3. Topological Binary Relationship

For satellite imagine, local rotational distortions are relatively small. In this application, the topological binary relationships between all pairs of detected IPs within a local conjugate image patch is used as the only binary constraint since point feature features are lack of structural relationship. For each pair of detected IPs of a local conjugate image patch, the topological binary distances are defined as:

$$D_{x_{ij}} = s_x \cdot |x_i - x_j| \tag{40}$$

$$D_{y_{ij}} = s_y \cdot |y_i - y_j| \tag{41}$$

where i, and j are detected IP identifications, x and y are IP coordinates, s_x and s_y are sampling scale factors. The sampling scale factors are defined as the ratio of the current camera ground sampling distance to the standard camera ground sampling distance of 275 meters. The sampling scale factor s_y defined along the image line direction always equals to 1, whereas the sampling scale factor s_x defined along the image sample direction generally equals to 1 except for the nadir camera. For the nadir camera, the ground sampling distance is 250 meter which makes $s_x = 250/275$. The topological binary constraints are defined as:

$$B_{x_{ij}} = \frac{\left|(D_{x_{ij}})_u - (D_{x_{ij}})_l\right|}{(D_{max})_x} \tag{42}$$

$$B_{y_{ij}} = \frac{\left|(D_{y_{ij}})_u - (D_{y_{ij}})_l\right|}{(D_{max})_y} \tag{43}$$

where $(D_{max})_x$ and $(D_{max})_y$ are a pre-defined constant maximum binary distances.

With in-exact consistent labeling, we use the weighted errors from the above factors to determine if a labeling is possible:

$$\sum_{(u_1, \ldots, u_N) \in T} w[u_1, \ldots, u_N, f(u_1), \ldots, f(u_N)] \leq \varepsilon \tag{44}$$

Note at labeling processing, both the accumulated pass error, and the current error and the future error are added together to determine if the current labeling is possible.

A last important factor in the evaluation function is the number of matching IPs. It is unlikely that

the total of *M* IPs from one conjugate image patch can all be matched with a subset of *N* IPs from another conjugate image patch. Therefore, even if one pairing is failed at a node of the search tree, we may want to continue to explore its descendents as long as there are some promising potential of matching in the future. Ultimately, we look for that particular matching branch out of that big number of total possible labeling branches. The final matching branch is defined by the path of the search tree from its root to the leaf with maximum number of consistent labelling.

Consistent Labeling Algorithm

Finally, the inexact consistent labeling algorithm for the IP matching is defined as:

```
Consistent_labeling_treesearch(
Unit_list, Unit_patch, Label_list, Label_patch, Binary_relation,
FTAB, Mch_fct);
Select the first unit in the remaining unit list;
Return an end search flag if no more unit is left in the list;
For each possible label to the current unit according to FTAB
   Call Forward_check to check the compatibility of the current
   labeling with possible future labeling;
   If number of current match plus number of future match is
   larger than Tn
      Update the unit list and FTAB;
      Update the match function;
      Call Consistent_labeling_treesearch to label the next unit
      in the remaining unit list;
   End If
End For
If no match for the current unit but this is still a promising
branch
   Assign NO_MATCH to the current unit
   Call Consistent_labeling_treesearch to label the next unit in
 the remaining unit list;
End If

Forward_check(
Ftab, Unit, Label, Unit_remain_list, Label_list, Unit_patch,
Label_patch, Binary_relation, number_future_match);
For each unit in the remaining unit list
   For each possible label according to FTAB
      Compute the compatibility error according to similarity of
```

```
      unit label attributes and binary relations
      Update Ftab
      If the compatibility error is less than Te
        Update the number of future match;
      End If
    End For
End For
```

Pair-wised Matching

Because of the obliqueness of MISR imaging from camera to camera, the two conjugate image patches from a forward camera such as Df and an aftward camera such as Ba will be fairly distorted one another. In order to increase the probability of successful matching, the matching cameras are paired with either the adjacent cameras resulting in 8 pairs of matching cameras (DaCa, CaBa, BaAa, AaAn, AnAf, AfBf, BfCf, CfDf), or the every other adjacent cameras resulting in 7 pairs of matching cameras (DaBa, CaAa, BaAn, AaAf, AnBf, AfCf, BfDf). There are total 15 matching camera pairs. Multiple matching for each camera provides us a good redundancy and a way to detect blunders and increase the matching reliability.

Image Search Window

For each pair of camera, an image search window is defined for initially pruning a number of non-potential labels for every unit. It is defined by two factors. The first factor is the approximate parallax according to the navigation error. These can be up to 10 pixels in either line or sample. This parallax itself consists of two parts. One is a constant bias representing the knowledge navigation error. The other is an additional error representing the worst possible error for this particular orbit segment. According to the definition of local conjugate image patches, there should not be any parallax between the conjugate image patches if there is no error in the navigation data. This means that the center of one of the conjugate image patch is the conjugate location of its conjugate image patch. With the presence of navigation errors, the constant bias will transfer the center of one image patch to an offset to the center of another conjugate image patch whereas the dynamic error may further lead this conjugate location off to an area around that offset location. We define the combination of the effects as the knowledge approximate parallax correction: $[l_0 \pm \Delta l, s_0 \pm \Delta s]$.

The second factor is the parallax caused by a combined effect of camera view angle difference and elevation difference. MISR cameras have the following nominal view angles along the swath: (70.5°, 60.0°, 45.6°, 26.1°, 0.0°, –26.1°, –45.6°, –60.0°, –70.5°) and a maximum 15° of side looking angle. The image disparity of a camera relative to the nadir view can be defined as:

$$p = \frac{h \tan\theta}{S}, \tag{45}$$

where h is the maximum surface elevation change in meters, θ is the camera view angle, S is the image sampling distance on the ground, and p is the image disparity in pixels. The search window is simply enlarged with a size of $(\delta l, \delta s)$ (both numbers are always positive). δl is the summation or the subtraction of the two image disparities relative to the nadir view depending on if the pair of conjugate image patches are from opposite view cameras (forward and aftward) or same view cameras (either forward or aftward). δs is half the disparity defined with the maximum side looking angle because the side looking angles for a pair of conjugate image patches are likely to be close.

Combining effects of both factors, the image search window is defined dynamically as: $[l_0 \pm (\Delta l + \delta l), s_0 \pm (\Delta s + \delta s)]$, where (l_0, s_0) is the image search window center offset and $(\Delta l + \delta l, \Delta s + \delta s)$ is the window size in line and sample. The image search window then varies from difference camera pairs, different surface condition, and different imaging condition. Note that the image search window is estimated according to our knowledge about the imaging condition and surface condition. Overestimating will result in a larger and maybe ambiguous search space. On the other hand, underestimating may miss some possible matching. However, this is not a sensitive parameter.

Unit Ordering

For a pair of local conjugate image patches, the one image patch with less detected IPs is selected as the unit image patch, the other one is the label image patch. The unit list and label list are then built with their attributes and binary relations computed. In order to minimize the unnecessary search, the unit list is ordered according to the number of potential match candidates. The number of potential match candidates is determined before the tree search according to the initial values from FTAB. In the initial FTAB, the error value in row m (the mth unit IP), column n (the nth label IP) is initialized only if the nth label is inside the image search window of the mth unit and this is a potential matching pair otherwise, the error value is simply assigned to be larger than T_e to indicate this is an impossible matching pair. Unit with less matching candidates is listed first to prune out a large portion of unnecessary search tree.

Combine Pair-wised Matching to TPs

Relational-based feature matching results 15 pairs of matching IP lists with matching accuracy close to a couple of pixels. Each list provides a pair of matching camera identifications and pairs of IP identifications from the two IP coordinate lists corresponding to the two matching cameras, respectively. Combining pair-wised matched IPs not only provides us an initial feature-base matched TP table but also a way to detect matching blunders. The algorithm used to combine pair-wised matched IPs to TP is an approach called determination of equivalent classes, details can be refereed to as reference [4]. It is important to check if all the matching pair are consistent one another in the building of the initial feature-base matched TP table. For example, (0, 4) is a pair of IP ids from the matching list of DfCf cameras, (0, 2) is a pair of IP ids from the matching list of DfBf cameras. We then result in a TP in the TP table as (tp_id = 0, Df = 0, Cf = 4, Bf = 2).

Now (4, 1) is a pair of IP ids from the matching list of CfBf cameras. The insertion of this new point will result in an in-consistency. Any in-consistency appeared during the building of TP table indicates potential blunders. Therefore, the process of combining pair-wise matched IPs is also a process to remove blunders occurred during the relational-based feature matching processing.

Area-based Precise Matching

Area-based matching algorithms measure the similarity of the image values in two local image windows around the matching points from the two images. Most of area-based matching techniques provide higher matching accuracy comparing with feature-based approaches but requiring good approximation priori the matching. That is why feature-based matching is applied first. The most commonly used area-based image matchers are cross-correlation coefficient maximum and least-square adjustment. Both matchers match a template window centered at the target point from one image with a sequence of correspondent windows in a search area of the search image. In order to avoid the error propagation, one template image patch is selected for the matching of multiple image patches. For each initial TP resulted the feature-based matching, the camera whose IP is the most distinct according to interest values of the initial conjugate IPs is selected as the template camera. Remind that the interest value of the Forstner's interest operator describes the distinctness of the detected point features like corner or center of image value gravity.

Cross-Correlation Coefficient Maximum Matching

In order to provide reliable Cross-correlation coefficient maximum (CCORR) in the case of multiply matching of distorted image viewed with large angle differences, the following conditions are applied with CCORR:

1. Image matching only applies on absolute cloud free condition (clear with high confidence).

2. The resulting location from cross-correlation coefficient can only be located within ± 2 pixels around the input IP location.

3. The maximum cross-correlation coefficient must be larger than a pre-defined threshold, and the average of the eight direct neighborhood pixels around the maximum pixel must also be locally large indicating the center pixel is on the hill of a cross-correlation coefficient surface in order to ensure the reliability.

4. Assuming the maximum cross-correlation coefficient location is found correctly with the above insurant condition, the hill of cross-correlation coefficient surface is represented by a quadratic two-dimensional polynomial. The top of the cross-correlation coefficient hill is then located at the maximum of this polynomial and be used as the CCORR match location. This step increases the accuracy of CCORR to up to one third of a pixel.

According to [5], let a two-dimensional symmetry index set be $I = \{-1, 0, 1\} \times \{-1, 0, 1\}$ and a

two-dimensional discrete orthogonal polynomial set be

$$\{p_n(x, y), n = 0, \ldots, 8\} = \{1, x, x^2 - 2/3\} \times \{1, y, y^2 - 2/3\} \tag{46}$$

over a 3 x 3 window. Let $C(x, y) = a_0 + a_1 x + a_2 y + a_3 x^2 + a_4 xy + a_5 y^2$ be the cross-correlation values over the same window. The least-square fitting of it can be resulted by minimizing:

$$e^2 = \sum_{x, y \in win} \left[C(x, y) - \sum_{n=0}^{8} k_n p_n(x, y) \right]. \tag{47}$$

Due the orthogonal property of the discrete orthogonal polynomial, we have:

$$k_n = \sum_{x, y \in win} w_n(x, y) C(x, y) \tag{48}$$

where $w_n(x, y)$ is called the kernel weight and can be calculated as:

$$w_n(x, y) = p_n(x, y) / \left(\sum_{x, y \in win} p_n^2(x, y) \right) \tag{49}$$

The cross-correlation coefficient maximum is determined at the location:

$$(x, y)_{match} = \left\{ \left(\frac{\partial}{\partial x} C(x, y) = 0 \right), \left(\frac{\partial}{\partial y} C(x, y) = 0 \right) \right\} \tag{50}$$

Least-Square Matching

Least-square matcher (LSM) is applied to the result of the cross-correlation coefficient matcher. Due to the distortion from camera to camera, the initial approximate conjugate locations has to be very close to the truth. The same template camera is used. The least-square template window is larger than that of the cross-correlation coefficient matcher, currently set at 13 x 13. The larger template window is used to increase the reliability. On the other hand, the allowable search window is smaller. The moving of the correspondent window is only allowed to be shifted about one pixel from the initial location. The σ for LSM is less than one fifth of a pixel.

The goal of area-based precise matching is to match TP with high accuracy for all 9 cameras for each set of local conjugate image patches. Sometimes it takes a group of TPs to match successfully with LSM for all 9 cameras. For example, TP one matches with LSM for camera Df, Cf, Af, An, Ba and TP two matches with LSM for camera Cf, Bf, Aa, Ba, Ca, Da. For both TPs, the final

TP locations for the cameras not matched with LSM are matched with either CCORR, or feature-based matcher, or just initial IPI locations, depending on if CCORR, or feature-based matching has succeeded at the point. Each TP, however, is required to be precisely matched with LSM at a pre-defined minimum number of cameras. Note that the matching accuracy decreases in the order of LSM, CCORR, feature-based matching, IPI.

Output

A set of image point measurements representing tie points, and associated variance-covariance matrix. Each TP also has an approximate ground coordinate with a variance-covariance matrix. The structure of this output is identical to the one from GCP identification.

3.4.2.3 Simultaneous Bundle Adjustment

Objective

The navigation and attitude data may contain errors which could, when propagated, reduce the accuracy of the geo-location and co-registration to an unacceptable level. The goal of "Simultaneous Bundle Adjustment" is to model and estimate time-dependent error functions. When used with the already supplied navigation and attitude data and in-flight calibrated CGM, during forward projection, these error functions will assure pointing with acceptable accuracy.

Input

1. In-flight calibrated CGM
2. List of GCPs associated with the orbit path of interest.
3. List of tie points extracted from MISR imagery associated with the orbit path of interest.
4. DID.
5. Supplied navigation and attitude data.

Mathematical Description

The basic ideas characterizing this approach are as follows:

a) Take advantage of MISR multi-viewing capability: at an instant of time the MISR instrument observes (simultaneously) nine different locations on the ground. Consequently, a single ground point is seen at nine different instants of time. Through the use of tie points a strong connection between discrete navigation and attitude data can be made, so that estimation of a time dependent error function is feasible. This was described in §3.4.2.2.

b) Model the attitude and ephemeris knowledge errors according to a physical model of the measurement devices.
c) Use the DID as a constraint for the adjustment.
d) Use available GCPs as a constraint for the adjustment.
e) Use a nonlinear least squares technique to determine the best fit of the parameters of attitude and ephemeris error model.
f) Do blunder detection using data snooping techniques.
g) During initial testing of the system, evaluate how well our orbit measurement model models the real EOS-AM1 orbit.

Ephemeris Measurement Model

The TDRSS Onboard Navigation System (TONS) is used to produce estimates of the EOS-AM1 ephemeris at 10.24 second intervals, during those times that contact with the TDRSS can be established. In between estimates from TONS, a real-time interface algorithm is used to propagate the ephemeris.

Contact with the TDRSS satellite can not be maintained throughout the whole EOS-AM1 orbit. There are two contacts per orbit, each lasting for about 10 minutes. During other times, the real-time interface algorithm is used to propagate the ephemeris forward in time.

The largest ephemeris errors occur during the times between TDRSS contacts. The most important error term in the real-time interface algorithm is a drag term that is not fully accounted for. This error term leads to errors mostly in the along track direction, and is close to linear in time.

This gives the following measurement model:

$$X_{OCS}^{measured} = X_{OCS}^{true} + a(t - t_0) + b \tag{51}$$

The measurement model for $Y_{OCS}^{measured}$ and $Z_{OCS}^{measured}$ are identical. Note that this is done in the orbital coordinate system, so that $Z_{OCS}^{measured}$ is in the radial direction, $X_{OCS}^{measured}$ is in the along track direction, and $Y_{OCS}^{measured}$ is in the cross track direction.

Attitude Measurement Model

The attitude of the EOS-AM1 spacecraft is measured by a combination of two instruments, a pair of solid state star trackers (SSST) and an inertial reference unit (IRU), made up of three gyros and an associated computer. A fine sun sensor (FSS) is used as a backup if one of the SSSTs fails.

The attitude is determined by a Kalman filter. The filter is updated every 10 seconds, if SSST or FSS sensor measurements are available. The filter updates a six-element state vector consisting of three small angle attitude errors and three gyro bias compensation errors. At other times, the attitude is propagated using the IRU.

The two SSSTs will generally see a star every 10 seconds. However, under certain circumstances there can be substantial interference by the moon, preventing a filter update for as long as 20 minutes. If the FSS is being used because one of the SSSTs fails, measurements of the sun will be made every 10 seconds while the sun is visible. However, the FSS can only be used for about 22 minutes out of the 90 minute orbit.

Between the SSST/FSS measurements, the IRU is used to determine the attitude rates. The IRU consists of three rate-integrating gyros operating in a torque rebalance strap-down mode. The gyro rates are measured every 0.128 seconds, and the attitude and rates are updated every 0.512 seconds.

The star tracker measurement is modeled as:

$$A_{\text{measured}} = A_{\text{true}} + E_{\text{static}} + E_{\text{dynamic}} \tag{52}$$

Where A refers to one of the attitude angles; roll, pitch, or yaw.

The IRU measurement is modeled as:

$$\Delta A_{\text{measured}} = \Delta A_{\text{true}} + E_{\text{bias}} + E_{\text{gyro white noise}} \tag{53}$$

We can combine the two measurement models to give:

$$A_{\text{measured}} = A_{\text{true}} + E_{\text{attitude}} \tag{54}$$

Where E_{attitude} is slowly varying, changing on the scale of tens or hundreds of seconds. We will examine this term more closely in the following sections.

Sensitivity to Attitude Errors

Before describing how to model E_{attitude}, we first will examine the sensitivity of determining camera pixel locations to errors in the attitude. Using a nominal set of camera parameters, a program was written to determine the change in pixel location for a change in the attitude for each of the nine MISR cameras. The results are shown in Table 3.

Table 3: Sensitivity to Attitude Errors (camera pixel 0, red band)

Camera	Yaw + 10 arcseconds		Pitch + 10 arcseconds		Roll + 10 arcseconds	
	Along track (meter)	Cross track (meter)	Along track (meter)	Cross track (meter)	Along track (meter)	Cross track (meter)
DF	-21	-65	228	-22	-33	46

Table 3: Sensitivity to Attitude Errors (camera pixel 0, red band)

Camera	Yaw + 10 arcseconds		Pitch + 10 arcseconds		Roll + 10 arcseconds	
	Along track (meter)	Cross track (meter)	Along track (meter)	Cross track (meter)	Along track (meter)	Cross track (meter)
CF	-16	-47	123	14	-20	41
BF	-12	-30	67	-7	-11	39
AF	-11	-15	42	-3	-5	38
AN	-9	-1	34	3	0	41
AA	-10	15	42	8	4	38
BA	-10	30	70	14	8	39
CA	-10	47	122	22	12	41
DA	-11	67	247	35	17	44

As can be seen, we are not equally sensitive to each of the attitude angles. We are far more sensitive to pitch than any of the other angles. The effect of yaw and roll are roughly the same, and are largely in the cross track direction.

Attitude Error Model

The error term E_{attitude} is a slowly varying function. We intend on modeling it by a spline curve. The spline is a piecewise cubic polynomial, with coefficients selected so that the value of polynomial and its derivative at the location of the knots match the given position and velocity of the knot. For the polynomial valid between knot i and $i+1$ with angle at t_i of a_i, rate at t_i of a_i' and an angle and rate at time t_{i+1} of a_{i+1} and a'_{i+1} we have:

$$a = c_0^i + c_1^i \frac{t - t_i}{t_{i+1} - t_i} + c_2^i \left(\frac{t - t_i}{t_{i+1} - t_i} \right)^2 + c_3^i \left(\frac{t - t_i}{t_{i+1} - t_i} \right)^3 \tag{55}$$

$$c_0^i = a_i \tag{56}$$

$$c_1^i = a_i'(t_{i+1} - t_i) \tag{57}$$

$$c_2^i = 3(a_{i+1} - a_i) - (a'_{i+1} + 2a_i')(t_{i+1} - t_i) \tag{58}$$

$$c_3^i = -2(a_{i+1} - a_i) + (a'_{i+1} + a_i')(t_{i+1} - t_i) \tag{59}$$

The location of knots in the spline are determined so that the resulting spline models the attitude error closely enough to meet the error budget for the simultaneous bundle adjustment. As shown in the last section, our sensitivity to pitch is much larger than to yaw and roll. This suggests that we actually want to use a different spacing of knots for each of the attitude angles; we can tolerate fewer knots for the yaw and roll.

We intend on using equal spaced knots, with the spacing adjusted to give acceptable accuracy of the attitude. However, a specific knot might not have enough tie points or sufficient camera coverage around it to determine the knot parameters. We remove knot i if:

$$\sum_{\text{cameras}} N_{\text{tie point seen}}(t_i, t_{i+1}, \text{camera}) < \text{Threshold} \tag{60}$$

or

$$\sum_{\text{camera}} \{1 \text{ if } (N_{\text{tie point seen}}(t_i, t_{i+1}, \text{camera}) \neq 0), 0 \text{ otherwise}\} < \text{Threshold} \tag{61}$$

Collinearity Constraint

Each tie point i has a position on the ground P_i, as well as a covariance matrix describing the uncertainty of that position. In addition, the location of the tie point in the image of each of the cameras j where the tie point is seen is given, which we will call I_i^j. A covariance matrix gives the uncertainty of the image location.

We can connect the location of the tie point with the ephemeris and attitude model by making the constraint that the image location predicted by the ephemeris and attitude should match the actual image location. The image location predicted by the ephemeris and attitude model is determined by the Image Point Intersection (IPI) algorithm (see [M-10]).

This leads to the following series of equations:

$$I_i^j = IPI^j(P_i, \text{Ephemeris parameters, Attitude parameters}) \tag{62}$$

In general, this system of equations cannot be solve exactly, so the equality should be taken in a least squares sense, weighted by the covariance matrix of I_i^j. When solving this system of equations, we let the location P_i and the ephemeris and attitude parameters vary, scaled by their respective covariance matrixes.

Surface Constraint

While varying the location of P_i, we want to take advantage of the fact that we have a description

of the surface. Since we know a tie point is going to lie on a surface, we add the following to our series of equations:

$$h_{DID}(P_i) = h_{\text{above WGS84}}(P_i) \tag{63}$$

Again, this set of equations are to be taken in the least squares sense, weighted by the uncertainty of the DID.

Ground Control Point (GCP) Constraint

We have collected a set of GCPs for camera calibration (see §3.3.4), which we want to take advantage of during the simultaneous bundle adjustment. We treat the GCPs as any other tie point, using a system of equations like (62) to impose the collinearity constraint. In addition, we want to constrain the location of P_i to the known location of the GCP P_i^{GCP}. We do this by adding the following to our series of equations:

$$P_i^{GCP} = P_i \tag{64}$$

Again, this equation is to be taken in the least squares sense, weighted by the covariance matrix of the GCP location.

Solution of System of SBA Equations

We solve the nonlinear system of equations (62), (63), and (64) by using the standard Levenberg-Marquardt method (see [4]).

The Levenberg-Marquardt method is used to minimize $F^T(x)WF(x)$. In our particular example, F is the right side of the equations (62), (63), and (64) minus the left side. W is the weight matrix, which is the inverse of the covariance matrix. The algorithm is iterative, calculating new value of x by:

$$x_n = x_{n-1} - (J^T(x_{n-1})WJ(x_{n-1}) + \lambda I)^{-1} J^T(x_{n-1})WF(x_{n-1}) \tag{65}$$

where J is the Jacobian and λ is a parameter controlling how large of a step we make take in the steepest descent direction. The algorithm iterates until a stopping criteria is reached, such as having the residuals $F(x_n)$ being sufficiently small.

The covariance of the resulting parameters is given by

$$C = (J^T(x_{n-1})WJ(x_{n-1}) + \lambda I)^{-1} \tag{66}$$

Sparsity of Jacobian

The Jacobian is a sparse matrix. There are many zeros in it. For instance the derivative of a equation dealing with a tie point with the spline coefficients is zero for the splines covering times that the tie point is not seen by one of the camera. Significant savings in time and memory can be achieved by taking advantage of the sparsity of the Jacobian.

The algorithms for solving sparse systems are a well developed field. Rather than developing special techniques for dealing with the specific Jacobian, a general direct solver will be used. This is available from a third party library. The algorithms used by this library are described in [20].

Blunder Detection

It will be the case that some of the tie points collected will have incorrect data, because the tie point was incorrectly located in one of the camera images. We also expect to have errors in the DID used to determine the surface constraint equation (63). It is also possible that the location assigned to a GCP in equation (64) is incorrect, only this is not expected to occur (it would indicate an error in our process of collecting GCPs). We would like to recognize these blunders, and remove their incorrect contribution to the simultaneous bundle adjustment.

The technique we use to detect blunders is data snooping. This is very similar to the blunder detection algorithm in [M-10], and the reader is referred to that document for a more complete description of the theory behind this algorithm.

After determining the parameters that best fit a system of equations, we calculate the standardized residuals of each of the equations. If the standardized residual is greater than a threshold value (e.g., 3), then the equation is marked as potentially containing a blunder. The response to this depends on the type of equation:

1. For a collinearity constraint equation (62), mark the image point in the tiepoint for the camera angle appearing in the equation as invalid. If this reduces the number of camera angles that the tie point is seen below a threshold, then mark the entire tiepoint as invalid.

2. For a surface constraint equation (63), we assume that the DID is incorrect. Remove the surface constraint equation from the system of equations to be solved.

3. For a GCP constraint equation (64), we assume that the location of the GCP is incorrect. Remove the GCP constraint equations from the system of equations, along with the collinearity and DID equations associated with the same point. Note that this is an unexpected blunder, and could indicate an error in our process of collecting GCPs. So in addition to removing the GCP equations, an error message should be printed out so that we can investigate the problem more careful and determine if there actually was an error in the GCP.

We start with the potential blunder with the largest residual. The equations affected by the potential blunder are removed, and the best fit to the parameters are recalculated. We compare the estimated standard deviation before and after the removal of the potential blunder against a threshold:

$$\frac{\hat{\sigma}_{i+1}}{\hat{\sigma}_i} < \text{Threshold} \tag{67}$$

If this test is met, we then assume that the potential blunders actually was a blunder a, and repeat the process of blunder detection on the new system of equations. Otherwise, we assume that the potential blunder wasn't a blunder. We replace the equations that were removed, and then test the potential blunder with then next largest residual. We continue this process until there are no remaining potential blunders.

Evaluating the Orbit Measurement Model

During the initial testing of the SBA system, we will evaluate how well the orbit measurement model described earlier works in practice. There are two aspects of the model to be evaluated. One is the determination of what time interval should be used between knots in the each of the attitude splines. The second is an evaluation of entire approach to modeling the orbit; does it do an adequate job to meet the overall geolocation and registration requirements? For example, is the linear position model adequate, or should we use something more complicated such as a spline?

Determining knot spacing

There are two competing goals in determining the knot spacing in the attitude splines. On the one hand, we want the knots as close together as possible to allow the maximum ability to model rapid changes in the attitude error. On the other hand, we want the knots to be as far apart as possible to improve robustness, since we have more tie points in a larger time interval and are therefore less sensitive to a single blunder, and processing time, since we have a smaller number of parameters to solve for.

To determine the optimum knot spacing, we will do the following:

1. Perform SBA to get an improved estimate of the ephemeris and attitude data using the smallest reasonable time spacing. The small time spacing is the one that allows us to get a minimum number of tie points in each time interval. Right now, we estimate the smallest time spacing at 10 seconds.

2. Repeat the SBA, using larger time spacing.

3. Compare the resulting orbit from the smallest time spacing with the one for a larger time spacing, by plotting the difference in the ephemeris and attitude data. By using the sensitivity data in Table 3, we can convert these differences to a difference in geolocation. This is an estimate

of the geolocation error induced by using the larger time spacing.

4. Repeat steps 2 and 3, until we determine the largest time spacing that has an acceptable geolocation error.

Note that the knot spacing is determined independently for each of the attitude angles. As shown in Table 3, we are much more sensitive to pitch than to either yaw or roll. So it will likely turn out that the time spacing between knots needed for the pitch spline will be much shorter than the time spacing needed for either yaw or roll.

Evaluating approach to modeling orbit

To determine how well the orbit model describes the real model, we will use GCPs as checkpoints. We will do the following:

1. Select a particular path as the one to be tested (e.g., one going over North America). For this path, collect a large number of well distributed GCPs, determining their geolocation through some other process (see §3.3.4).

2. Perform the tie point extraction using the full set of GCPs, but perform the SBA using only a small subset of the GCPs. We should select the number of GCPs that will be seen in a typical path.

3. Determine the location of the GCPs in the imagery by doing an Image Point Intersection using the orbit model resulting from the SBA, and compare to the locations determined by image matching during tie point extraction.

The residuals of the comparison give a direct measurement of the error in geolocation by using the orbit determined by the SBA. This in turn gives a measure of how well the orbit model describes the true orbit.

If the error in geolocation is in the error budget, we accept the orbit model. Otherwise, we will need to develop a better one.

Problem Size

An important quantity to consider is the size of the Jacobian. We don't yet know how frequently we need to place knots in the attitude splines in the orbit model, or how many tie points we are using. However, we can come up with a reasonable limit on the order of magnitude of the problem (i.e., are we talking about 100 parameters, or 1,000,000?).

There are 2 parameters in equation (51) for each of the three ephemeris measurements, fora total of 6 parameters. There are 2 parameters for each knot in the attitude splines for each attitude angle

in equation (54). Finally, there are three position parameters for each tie point, appearing in equation (62). This gives the following number of parameters:

$$6 + 2N_{\text{yaw knot}} + 2N_{\text{roll knot}} + 2N_{\text{pitch knot}} + 3N_{\text{tiepoint}} \tag{68}$$

For each tie point we get one surface equation (63). For each camera angle that the tie point is seen in, we get two equations (62) (one for image line and one for image sample). Finally, for each tie point that is also a ground control point we get 3 equations (64) (one for each coordinate). This gives the following number of equations:

$$2\sum_{i} N_{\text{camera angle for tiepoint i}} + N_{\text{tiepoint}} + 3N_{\text{GCP}} \tag{69}$$

The attitude Kalman filter on the EOS-AM1 spacecraft is updated every 10 seconds. As on upper limit on the knots, lets say that we space the knots every 10 seconds[1]. This gives a total of

$$N_{\text{knot}} = \frac{T_{\text{day side}}}{T_{\text{knot spaciing}}} \approx \frac{\frac{T_{\text{orbit}}}{2}}{T_{\text{knot spacing}}} = \frac{\frac{(98)(60)}{2}}{10} \approx 300 \tag{70}$$

For each spline knot, we have 2 parameters that need to be fitted for, for each angle. This gives an upper limit of 3 x 2 = 6 parameters per 10 second interval. A tie point is seen during more than one time interval, so the 3 parameters appearing in equation (68) don't need to fully accounted for in one time interval. As an estimate, we add one parameter for each tie point. So we need

$$6 + \sum_{\text{camera}} N_{\text{tiepoints seen}}(t_i, t_{i+1}, \text{camera}) \tag{71}$$

equations. This requires just 6 tie point to be seen in the time interval between knots. We want some redundancy, so as an order of magnitude estimate lets say that we want to see 10 tie points in each time interval. As an estimate, lets say each tie point is seen at 5 different camera angles. This gives about 600 tie points over an orbit. The number of GCPs will be relatively small, so we can safely ignore their contribution in (69), for purposes of getting an order of magnitude estimates.

Plugging the numbers in, we get an estimate for the upper size of the problem of about 6,600 equations, with about 3,600 unknowns.

1. Note, this is hardly a rigorous argument. We are trying to getting order of magnitude numbers here, so a hand waving argument like "use the same spacing as the Kalman filter" is acceptable.

3.4.2.4 Ground to Image Projection

Objective

The objective of this element of the in-flight geometric calibration is to actually produce "Projection Parameters" corresponding to a single orbit path. The goal is to combine results from the in-flight CGM calibration, simultaneous bundle adjustment, with the supplied navigation and attitude data and obtain the most accurate pointing of MISR pixel in order to geo-locate them. More specifically, previously defined grid points of the SOM map projection must be located in MISR imagery. Also, it must be determined if the ground point is terrain obscured for the imaging from certain MISR cameras.

Input

1. Nominal spacecraft navigation and attitude data

2. Global DTED Intermediate Dataset (DID)

3. Ancillary Geographic Product (AGP)

4. Pre-flight Camera Geometric Model

Mathematical Description

The whole operation can be broken up into the following parts:
a) The pointing directions of the imaging rays for several neighboring pixels are obtained.
b) The rays are traced down to the intersection with the surface.
c) The SOM grid point closest to one of the projected pixel is selected and subpixel location is obtained via a backward projection.
d) The percentage of obscuration for the selected grid cell is determined and grid point is flagged if necessary.
e) The selected grid point is projected back to the image, and its image coordinates are determined.

The details on some of the steps listed above (i.e., definition of the obscured pixel) are still being investigated.

Output

Pairs of coordinates giving the lines and samples in MISR image space corresponding to the map grid points of the predefined SOM projection. Also a list of flags, corresponding to the same points, indicating if the ground point is topographically obscured from the MISR camera.

3.4.2.5 Mosaic ROI

Objective

The ROI created to conform with the PP will provide capabilities to reduce errors from supplied navigation and attitude during autonomous georectification process. Prior to its rectification incoming MISR imagery will be corrected via image matching with the available ROI as described in [M-10]. However, it is reasonable to expect that a continuous ROI corresponding to an orbit path can not be made from a single orbit pass due to the large cloud cover. Therefore, the goal of this operation is to merge several cloud free ROI and resampled them to conform to same image space as the PP, creating a continuous composite with maximized cloud free percentage. The challenges are: a) identification of the cloudy and non cloudy imagery corresponding to the same region on the ground b) preservation of the spatial and radiometric accuracy while merging and resampling data from several orbit revolutions.

Input

1. Corrected spacecraft navigation and attitude data as the result from the simultaneous bundle adjustment.

2. L1B1 radiometrically corrected product.

3. In-flight calibrated Camera Geometric Model

4. Ancillary Geographic Product (AGP)

5. PP file

6. Radiometric Camera-by-Camera Cloud Mask (RCCM).

Mathematical Description

The creation of the single ROI (i.e., one camera, one orbit path) will take at least four L1B1 radiometrically corrected product in order to maximize cloud free percentage. Along with the L1B1 product a corresponding RCCM dataset will be used. In particular, creation of ROI will happen in four stages. Each stage deals with different pair of the L1B1 product and RCCM while ROI, and PP from previous stage are being updated. At the beginning, i.e., in the first stage ROI is a empty file and appropriate flags throughout PP are set to indicate condition of the non-available ROI. As the process go from stage to stage the amount of ROI is increasing and corresponding flags in the PP file will be set accordingly. Processing algorithm can be divide into three parts: 1) definition of image transformation between L1B1 product and image space of ROI, 2) resampling of the L1B1 product to the image space of ROI using previously defined transformation along with RCCM and PP flags which will indicate necessity of resampling, and 3) image histogram equalization

between available ROI and current L1B1 image in all stages after first one.

A. Definition of image transformation

Image transformation to be used is a modification of affine. Full derivation of this transformation model is given in [M-10] (pg. 4-9 to 4-11). For completeness, final equations (72) and (73) are given here:

$$s_{l1b1} = k_{14}(l_{roi} - l_0) + k_{15}(s_{roi} - s_0) + k_{16}(s_{roi} - s_0)^2 + k_{17}h_{surface} + k_{18} \quad (72)$$

$$l_{l1b1} = k_{19}(l_{roi} - l_0) + k_{20}(s_{roi} - s_0) + k_{21}(s_{roi} - s_0)^2 + k_{22}h_{surface} + k_{23} \quad (73)$$

where,

k_{ij} are transformation parameters,

s_{roi}, l_{roi}, s_{l1b1}, l_{l1b1} are coordinates of a conjugate point in ROI and L1B1 product respectively,

s_0, l_0 is a selected orgin in the area of ROI which is subject of transformation.

Parameters of the transformation k_{ij} are least-square estimated using coordinates of a two-dimensional array of tie-points. The tie-points are generated using the PP file as the road-map. In particular, a 5 x 10 grid of tie points is established over a SOM block of the PP ground space. Image coordinates of the tie points in the ROI image space are simple given by the PP values. Image coordinates of the tie points in the L1B1 product will be obtained using Image Point Intersection algorithm as described in [M-10] (pg. 4-20 to 4-23).

Resampling of L1B1 product to ROI

As in the previous part of algorithm, a SOM block of the PP ground space is use as the processing unit. Prior to actual radiance resampling the PP file combined with the RCCM is used to define candidate ROI image locations. In particular at each PP ground point flag indicating availability of ROI and corresponding RCCM flag are interrogated to define need for resampling. In the case of positive outcome (i.e., there is no available ROI and the point is cloud free) the first integer to the corresponding PP values is selected as the candidate location for resampling. It should be pointed out that selection of the candidate points must be enhanced in order to assure that each of the ROI image location has ben assigned a candidate or no-candidate status. Specifically, once the selection of the candidate points for a region is completed using PP file, the non assigned points take on the status of its neighbors. In the case of mixed status of surrounding points a candidate status

shall be assigned. As the following step, bilinear interpolation is used as the basis while computing new radiance. An ROI point (i.e., integer coordinates) falling somewhere in the L1B1 image, using relations (72) and (73), will have up to four surrounding points. For a given variable f that takes on values f_1, f_2, f_3 and f_4 at the surrounding points, the bilinear interpolated value is given by:

$$\langle f \rangle = (1-a-b+ab)f_1 + a(1-b)f_2 + b(1-a)f_3 + abf_4 \tag{74}$$

where a is the fractional distance $(0 \le a \le 1)$ of the interpolation point in cross-track direction and b is the fractional distance $(0 \le b \le 1)$ in the along the track direction, as shown in the Figure 9.

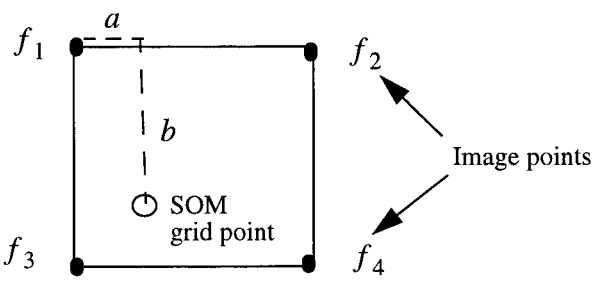

Figure 9: Bilinear interpolation

Once the resampling is finished corresponding PP flag must be changed to indicate availability of ROI for the future stage of ROI creation.

Histogram equalization

Prior to beginning of second and following stages in the creation of ROI a histogram matching between available ROI and current L1B1 imagery for the unit area (i.e., SOM block) must be performed by changing the values of the L1B1 image.

The goal of the ROI creation algorithm is to be fully autonomous while combining images of four or more orbit passes in order to maximize cloud free percentage. However, after each stage, with the help of customized image processing tools, ROI must be inspected interactively to verify reliability of the RCCM used.

Output

A composite of MISR L1B1 imagery constructed from several orbit passes.

3.5 ERROR BUDGET

3.5.1 Introduction

This section is the result of our effort to come up with an estimate of error associated with the geolocation provided through the paired Projection Parameters and Reference Orbit Imagery. Focus is on the part of algorithm (i.e., simultaneous bundle adjustment) designed to find a correction to the supplied navigation data which will allow creation of accurate reference projection parameters. For the purpose of the error analysis we implemented a simplified version of the final algorithm.

The model uses the least-square adjustment method in order to compute the correct position (X, Y, and Z) and attitude (roll, pitch and yaw), relative to the Orbital Coordinate System (see §A.1.5), at a specific instant of time. The condition equation, which represents our functional model, is collinearity as expressed by(10). Inputs to this model are: (1) coordinates of Ground Control Points (GCP), (2) image point measurements, (3) Camera Geometric Model (CGM), and (4) supplied (initial) navigation data. Output is corrected navigation data. In order to estimate errors of the corrected navigation data we include a stochastic model (i.e., statistical properties of all variables which are input to the functional model) into the adjustment. The realistic stochastic model is the basis for the meaningful variance-covariance error propagation. The one that we use represents a combination of the requirements imposed on some of the variables, and the assumptions based on previous experience.

The assumptions relative to the functional model are:

a) The corrections to the navigation data are computed at only one instant of time. The final version of the model, in contrast, will have a time dependent function representing correction to the navigation data.
b) Ground Control Points are used instead of DEM. The plan is to use only DEM in the final version.
c) The CGM are going to be somewhat different than ones used in this study.

The assumptions relative to the stochastic model are:

a) There are no errors in the CGM.
b) There are no errors in the GCPs.
c) There is a relatively large standard deviation associated with the image point measurement. The idea is to have these measurement with purposely larger error than expected in order to account for no simulation of errors in CGM and GCPs.

3.5.2 Functional model

Given the fact that MISR consists of nine cameras, a large number of combinations (number of cameras / number of Ground Control Points) may represent useful functional model. A functional

model is selected, out of many, which is believed to be the optimal one in regards to the precision of the corrected navigation data:

# of spacecraft positions = 1
# of cameras = 7 (tie points for all 9 cameras will not always be available)
# of GCP's = 3 per camera
image point measurements = 7x3 = 21

3.5.3 Stochastic model

As mentioned before, the stochastic model is based on the combination of requirements and our assumption or prediction. Requirements are used to set a priori standard deviation to the spacecraft position and attitude:

Position (X, Y, and Z; meters 1 sigma) --- 60.0, 60.0, 60.0
Attitude (roll, pitch, and yaw; arcsec 1 sigma) --- 20.0 20.0 20.0

The prediction, given all of the assumptions, is that a priori standard deviation for the image point measurement is going to be somewhere between 6 and 12 microns within the camera focal plane. Therefore, the results of the simulation are presented in two cases: Case I with the 12 microns, and Case II with the 6 microns.

3.5.4 Results of simulation

The results of simulation consist of errors in the navigation data before (Table 4) and after adjustment and estimated standard deviation of the corrected navigation data.

Table 4: Errors before adjustment

Position (meters)	-123.52	-95.58	-185.13
Attitude (arcsec)	-14.95	-61.21	-8.98

The estimated standard deviation of the corrected navigation data are computed through the variance-covariance error propagation as the part of least-square adjustment.

Case I, Table 5 and Table 6 (a priori standard deviation of image point measurement is 12 microns).:

Table 5: Errors after adjustment (Case I)

	X	Y	Z
Position (meters)	-87.53	-37.90	-82.13
	Roll	Pitch	Yaw
Attitude (arcsec)	-13.17	4.58	-1.94

Table 6: E posteriori estimate of Standard Deviation (Case I)

	X	Y	Z
Position (meters)	49.71	49.59	41.48
	Roll	Pitch	Yaw
Attitude (arcsec)	12.68	8.91	9.36

Case II Table 7 and Table 8 (a priori standard deviation of image point measurement is 6 microns):

Table 7: Errors after adjustment (case II)

	X	Y	Z
Position (meters)	-64.42	-8.61	-43.71
	Roll	Pitch	Yaw
Attitude (arcsec)	-11.53	-5.17	-0.57

Table 8: A posteriori estimate of Standard Deviation (Case II)

	X	Y	Z

3.0 REFERENCES

[1] Ackermann, F., Digital Image Correlation: Performance and Potential Application in Photogrammetry, Photogrammetric Record, vol. 11(64), 1984.

[2] Allen, C. W. Astrophysical Quantities, 3rd edition, Athlone Press, London, 1973.

[3] Castleman, K.R., Digital Image Processing, Prentice-Hall, N.J., 1979.

[4] Dennis, J. E. Jr and Schnabel, Robert B., Numerical Methods for Unconstrained Optimization and Nolinear Equations, Prentice-Hall, NJ., 1983.

[5] Diner, D., Atmospheric refraction, Interoffice Memorandum, MISR DFM #212, April 9, 1992.

[6] Gruen, A. W. and Baltsavias, E. P., High Precision Image Matching for Digital Terrain Model Generation, International Archives of Photogrammetry, vol. 25, no. 3, 1986.

[7] Hannah, M. J., Digital Stereo Image Matching Techniques, ISPRS 16th Congress, Commission III, Kyoto, Japan, 1988.

[8] Herrick, S,. Astrodynamics, Van Nostrand Reinhold, New York, 1971.

[9] Hochberg, E. B., Measurment of MISR camera pixel-theta characteristic, Interoffice Memorandum, MISR DFM #587, February 24, 1995.

[10] Forstner, W., On the Geometric Precision of Digital Correlation, ISPRS Int. Arch. of Photogrammetry, vol. XXIV, Commission III, Helsinki, 1980.

[11] Kaula, W., Theory of Satellite Geodesy: Application of Satellites to Geodesy, Blaisdell, 1966.

[12] Korechoff, R.P., Analysis of MISR Camera Geolocation and Registration Requirements, Interoffice Memorandum, MISR DFM #207 and OSA DFM #93-27, 1993.

[13] _____, Analysis of third breadboard CAT test,Interoffice Memorandum, MISR DFM #368, March 2, 1994.

[14] _____, CAT algorithm description, Interoffice Memorandum, MISR DFM #373, March 7, 1994.

[15] _____, MISR camera model, Interoffice Memorandum, MISR DFM #392, April 8, 1994.

[16] Larson. S., Software Implementation Guidelines, JPL D-10622, Version 2.0, January 1995.

[17] Leick, A., GPS Satellite Surveying, John Wiley & Sons, New York, 1990.

[18] Lewicki, S.A., M.M. Smyth, V.M. Jovanovic and E.G. Hansen, A simulation of EOS MISR Data and Geometric Processing for the Prototyping of the MISR Ground Data System, Procedings IGARSS'94 Symposium, vol. III, Pasadena, 1994.

[19] Mikhail, E. M., Observations and Least Square, Harper & Row, New York, 1976.

[20] Pissanetzky, S., Sparse Matrix Technology, Academic Press, Orlando, 1984.

[21] Snyder, J. P., Map Projection - A Working Manual, United States Geological Survey Professional Paper 1395, U. S. Government Printing Office, Washington, 1987.

[22] Steimle, L., MISR - Collimator Array Tool Calibration and Verification (the final Pre-Use Report), MISR DFM #562, January 18, 1995.

[23] Vanicek P. and Krakiwsky E. J., Geodesy: The Concept, Elsevier Science Publishers B. V., The Netherlands, 1986.

[24] Wertz, J., ed., Spacecraft Attitude Determination and Control, D. Reidel Publishing Company, Boston, 1978.

APPENDIX A: COORDINATE SYSTEMS

A.1 DEFINITIONS OF COORDINATE SYSTEMS

A.1.1 Detector Coordinate System

Figure 1 shows the placement of an arbitrary camera focal plane relative to a coordinate system called the detector coordinate system (DCS). The DCS x axis is defined to be perpendicular to the long axis of the detector arrays. The y axis is parallel to the long axis and is positive in the westward direction during a descending pass. The z axis is the cross product of x with y forming a right-handed coordinate system. As shown in Figure 1, the z axis intercepts the focal plane at the center of band 3. The figure also shows that the focal plane is located at z = -f where f is the effective focal length of the particular camera.

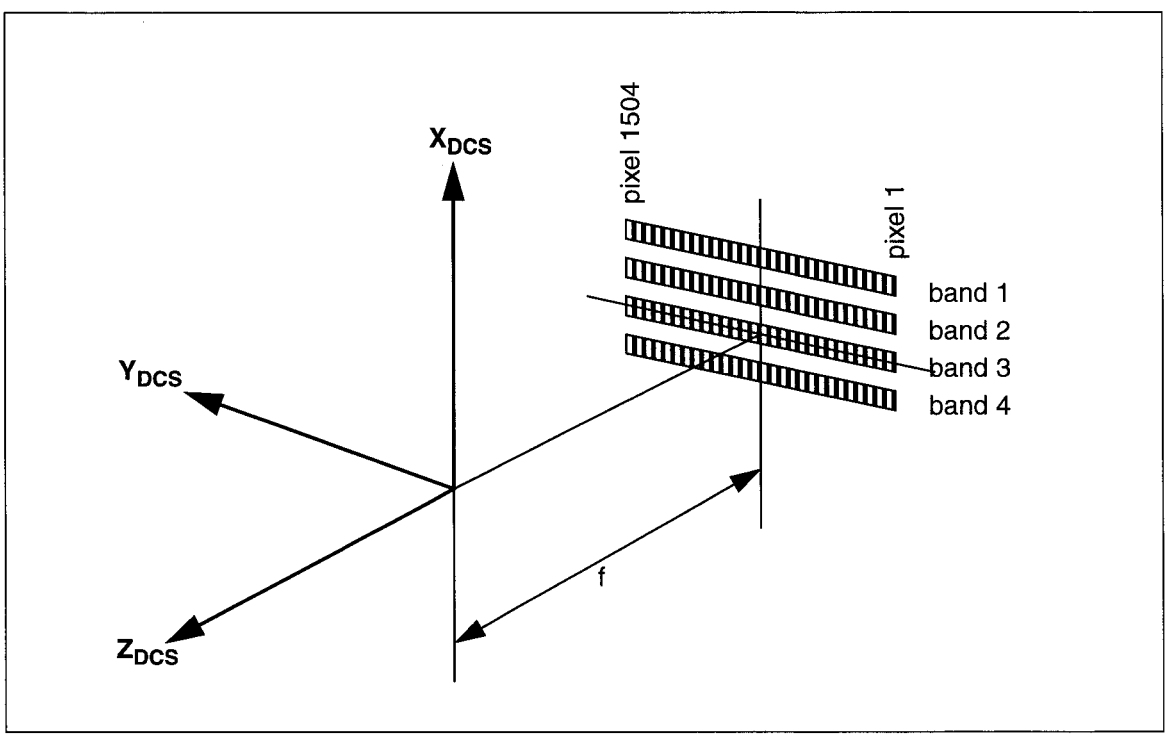

Figure 1: Definition of the Detector Coordinate System

A.1.2 Camera Coordinate System

In the camera coordinate system (CCS), the z axis is the mechanical symmetry axis of the camera barrel. The y axis is parallel to the long symmetry axis of the detector arrays and is positive in the westward direction during a descending pass of the satellite. The x axis is the cross product of the y axis and the z axis forming a right-handed coordinate system. Under ideal circumstances, the CCS is identical with the DCS. Due to fabrication and alignment errors, the DCS and CCS may

differ by small-angle rotations.

Physically, the plane formed by the intersection of the x and y axes is the interface between the camera and the optical bench, where the x axis is defined as passing through the center of the interface flange and the center of the pin and where the y axis is defined as lying in the plane of the locating pads perpendicular to the x axis. The z axis is then perpendicular to the lens barrel front flange.

A.1.3 Instrument Coordinate System

The instrument coordinate system (ICS) is a right-handed instrument coordinate system fixed relative to the MISR instrument with respect to reference surfaces (optical cubes) whose normals define the coordinate system. The pointing of each camera boresight (barrel mechanical axis) is defined in this coordinate system by two angles as shown in Figure 2. Each axis is nominally aligned with the corresponding axis of the spacecraft coordinate system defined below, and any differences will be the result of instrument mounting errors.

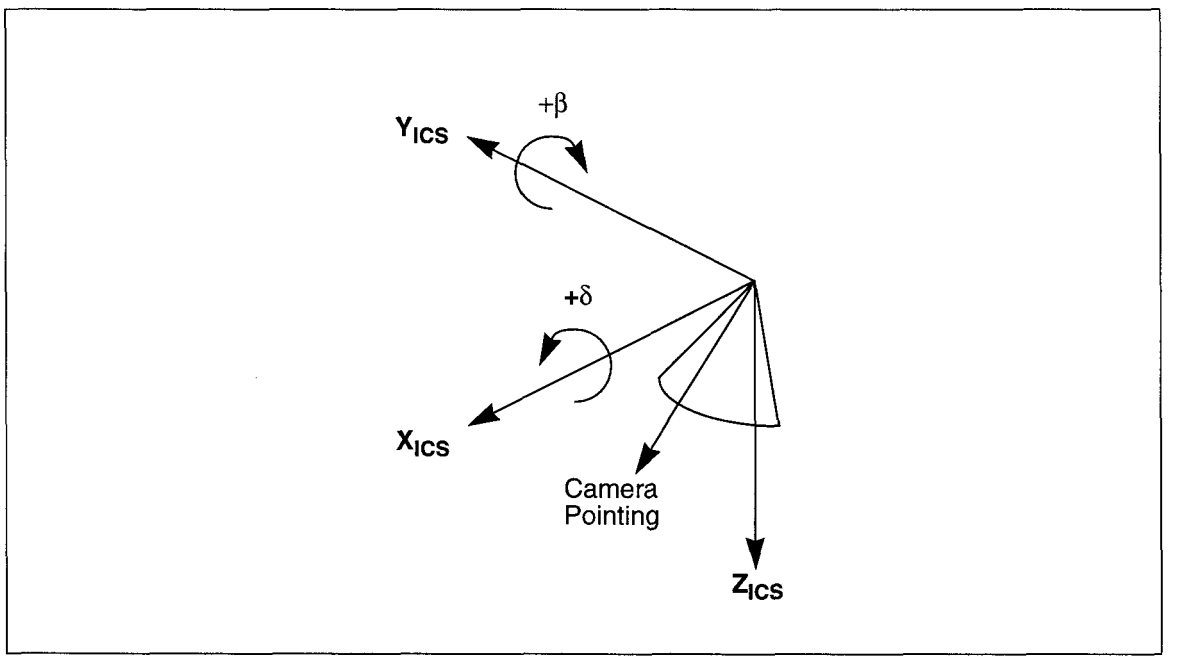

Figure 2: Definition of the Instrument Coordinate System

A.1.4 Spacecraft Coordinate System

The spacecraft coordinate system (SCS) and the ICS are nominally aligned except for a translation of the origin to the EOS spacecraft's center of mass. Misalignments between the ICS and SCS are due to fabrication errors or thermal effects. The SCS axes are fixed in relation to the spacecraft body. The relationship with the orbital coordinate system defined below is reflected through the attitude angles roll, pitch, and yaw. If those angles are all zero the two systems are identical.

A.1.5 Orbital Coordinate System

The orbital coordinate system (OCS) is a right-handed coordinate system with its origin at the spacecraft's center of mass (same as the SCS). The z axis is aligned with the spacecraft-to-Earth pointing vector. The y axis is defined by the cross product of the z axis and the EOS spacecraft velocity vector, and points toward the anti-Sun side of the spacecraft. The x axis is defined by the cross product of the y axis and the z axis. It points in the general direction of the spacecraft velocity vector, but is not necessarily instantaneously aligned with it due to Earth oblateness and eccentricity of the orbit. The rotations which transform the SCS into the OCS are defined by the attitude angles roll, pitch, and yaw.

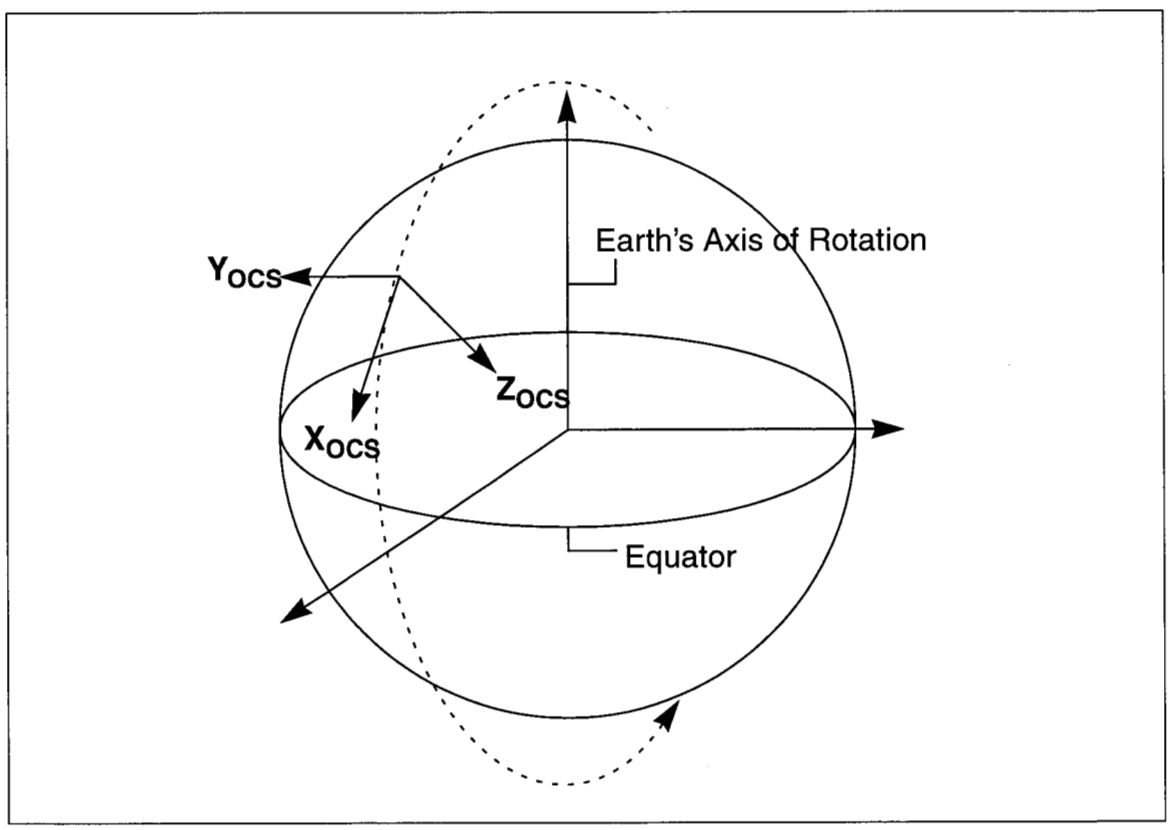

Figure 3: Definition of the Orbital Coordinate System

A.1.6 Geocentric Inertial Coordinate System

The geocentric inertial (GCI) coordinate system is a right-handed coordinate system defined to describe directions in an Earth-centered but not Earth-fixed frame. That is, the axes are defined with respect to directions in space and not with respect to locations on the Earth. The spacecraft position and velocity vectors are referenced to this coordinate system. The positive z axis is parallel to the Earth's rotation axis in the direction of the mean north celestial pole of epoch J2000.0 and the positive x axis points to the mean vernal equinox of epoch J2000.0. The y axis is the cross product of

the z axis and the x axis.

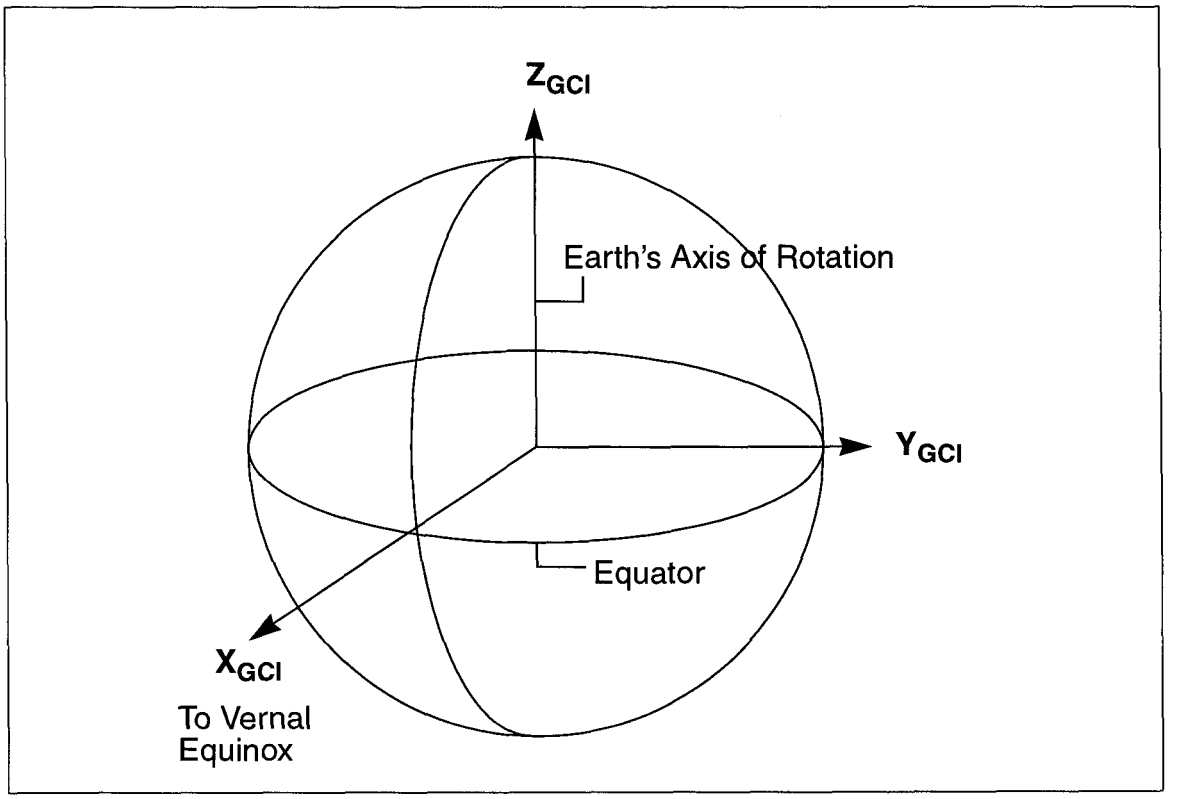

Figure 4: Definition of the Geocentric Inertial Coordinate System

A.1.7 Conventional Terrestrial Reference Coordinate System

The Conventional Terrestrial Reference (CTR) coordinate system is Earth fixed with its origin at the center of mass of the Earth. The coordinate system has been defined by the Bureau International de l'Heure (BIH), and it is the same as the U. S. Department of Defense World Geodetic System 1984 (WGS84) geocentric reference system. This coordinate system is defined in detail in reference [17]. The transformation from GCI to CTR accounts for precession, nutation, Earth rotation, and polar motion.

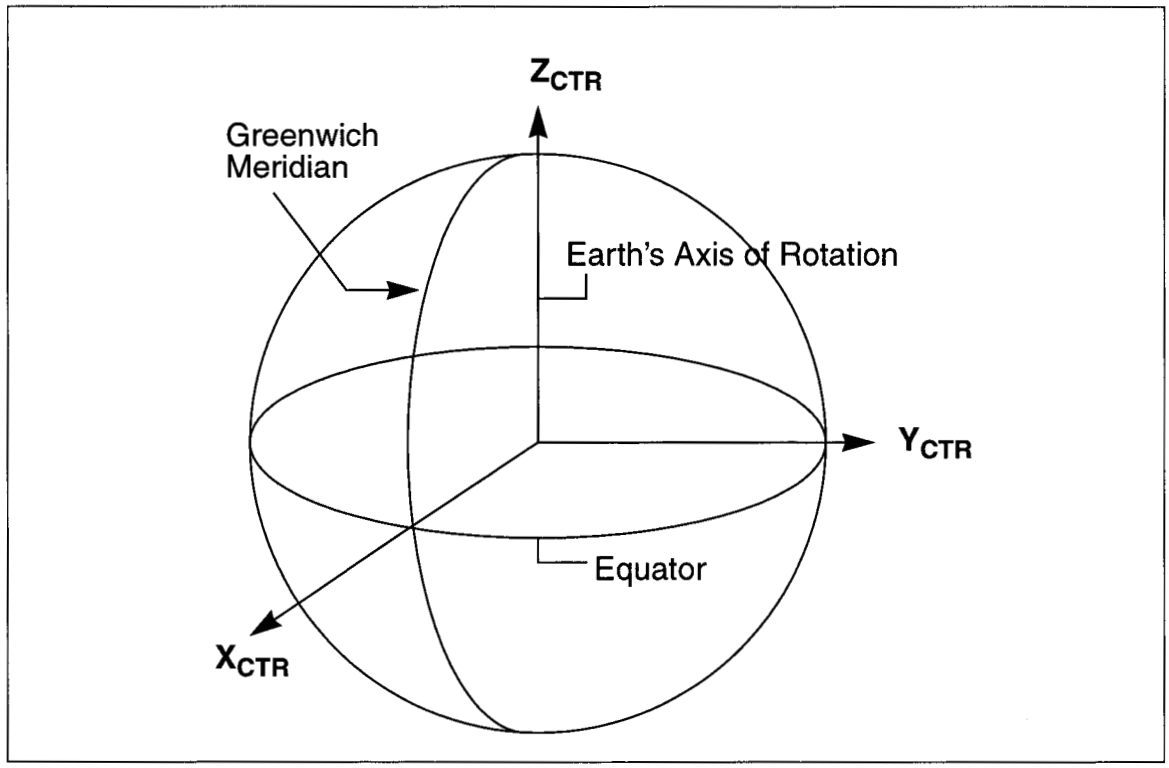

Figure 5:

A.1.8 Geodetic Coordinate System

The geodetic coordinate system is based on the WGS84 reference ellipsoid with coordinates expressed in latitude, longitude, and height above the reference Earth ellipsoid. Latitude and longitude are respectively the angle between the ellipsoid normal and its projection onto the equator, and the angle between the local meridian and Greenwich meridian, respectively.